

Review

Nanofiber-Based Materials for Persistent Organic Pollutants in Water Remediation by Adsorption

Elise des Ligneris ^{*} , Ludovic F. Dumée  and Lingxue Kong 

Institute for Frontier Materials, Deakin University, Geelong VIC 3220, Australia;
ludovic.dumee@deakin.edu.au (L.F.D.); lingxue.kong@deakin.edu.au (L.K.)

* Correspondence: e.desligneris@research.deakin.edu.au; Tel.: +61-035-227-3241

Received: 22 December 2017; Accepted: 17 January 2018; Published: 24 January 2018

Abstract: Fresh water is one of the most precious resources for our society. As a cause of oxygen depletion, organic pollutants released into water streams from industrial discharges, fertilizers, pesticides, detergents or consumed medicines can raise toxicological concerns due to their long-range transportability, bio-accumulation and degradation into carcinogenic compounds. The Stockholm Convention has named 21 persistent organic pollutants (POP) so far. As opposed to other separation techniques, adsorption, typically performed with activated carbons, offers opportunities to combine low operation costs with high performance as well as fast kinetics of capture if custom-designed with the right choice of adsorbent structure and surface chemistry. Nanofibers possess a higher surface to volume ratio compared to commercial macro-adsorbents, and a higher stability in water than other adsorptive nanostructures, such as loose nanoparticles. This paper highlights the potential of nanofibers in organic pollutant adsorption and thus provides an up-to-date overview of their employment for the treatment of wastewater contaminated by disinfectants and pesticides, which is benchmarked with other reported adsorptive structures. The discussion further investigates the impact of adsorbent pore geometry and surface chemistry on the resulting adsorption performance against specific organic molecules. Finally, insight into the physicochemical properties required for an adsorbent against a targeted pollutant is provided.

Keywords: nanofibers; adsorption; organic pollution; persistent organic pollutant POP; adsorption mechanisms; adsorbent characteristics; surface chemistry; pesticides; disinfectants; phenol

1. Introduction

Organic water pollution from synthesized chemical pesticides has been increasing over the past 50 years [1]. As a counter-measure, 21 non-polar organic molecules have been classified as persistent organic pollutants (POPs) by the Stockholm Convention (2001, 2017), to be banned or restricted globally [2]. Organochlorines (OCs) account for a large group of POPs, including aldrin or DDT pesticides, but also industrial chemicals such as the family of polychlorinated biphenyls (PCBs), as well as byproducts [1]. The list of POPs also includes several organophosphorus (OPs) pesticides, and among recently added compounds, flame retardants and polyaromatic hydrocarbons (PAHs) [1,2].

The release of POPs is associated with major toxicity concerns for both the environment and human health [3,4]. Their partial degradability affects the chemical oxygen demand (COD) of streams, causing oxygen depletion by consuming oxygen at a greater rate than its replenishment [4]. For some POPs, such as Heptachlor, it is the compound formed after reaction in water, Heptachlor epoxide, that causes threat to human life [5]. The persistency of POPs in the environment can be measured by their half-life duration (DT50). For instance, organochlorine DDT pesticide has a DT50 that, depending on the environment, ranges from 2 to 15 years [6]. The presence of POPs in the environment also affects human health, through the ability of POPs to bio-accumulate in organisms and bio-magnify

throughout the food chain [3]. Exposure of humans to POP can eventually occur through drinking water, via the leaching of pollutants from treated soil into aquifers. Detected levels of POPs in human blood were shown to lead, in some scenarios, to reproductive disorders, immune system alteration, and/or increased risk of cancer [3].

Long-range transportability is another concern associated with POPs [7–9]. As most POPs are semi-volatile compounds, they are able to cycle among air, water and soil [8]. Characteristics such as subcooled liquid vapour pressure and octanol-water ($\log K_{ow}$) partition coefficients, the latter defining the molecule hydrophilicity as well as temperature of condensation, enable the determination of the mobility of a persistent pollutant through a transportation cycle in the atmosphere, ocean or soil [7,8]. Warm temperatures, as experienced in tropical regions, enable the evaporation of POPs, while colder temperatures, at higher latitudes, enable the deposition of POPs from the atmosphere onto the ocean or continent [7]. POPs emitted in tropical to temperate regions may therefore be transported to one of the Earth poles, via successive evaporation–deposition cycles, also called the grasshopper phenomenon, determined by seasonal temperature changes at temperate latitudes. POPs emitted at high latitudes, however, are less subject to mobility due to lower temperatures [7]. Polar regions therefore act as an environmental sink for POP compounds [7,9]. However, as global warming is strongly affecting the polar climate, the possibility of a reverse in the deposition cycle of POP raises concerns [9].

To limit the environmental sink effect, local removal techniques must be put in place to remove pesticides from water. Advanced oxidation processes (AOP), including ozonation, enzyme digestion or catalysis, have been sought after to combine efficiency and fast kinetics [10–12]. These processes offer to date the most efficient alternative to conventional treatments, in terms of reduction of the total organic carbon (TOC) count in contaminated effluents. Several reviews cover the organic pollutant water decontamination via AOPs and provide a performance benchmark for this study [11,12]. The main roadblock to the implementation of AOPs is the increase of the effluent toxicity after treatment. For instance, the catalytic degradation of the triazine molecule Atrazine may release carcinogen amine groups in water [13]. Adsorption has been considered an alternative method of capture and removal of pesticide molecules from wastewaters [4]. Even though lower decreases in water TOC have been obtained by adsorption compared to AOPs, the effluent toxicity after treatment is still undetermined. However, there is a need for a specific adsorbent material able to combine over 95% removal efficiency, fast kinetics, recyclability and low fabrication cost.

Among common materials, activated carbons have been widely used against organic compounds and showed high adsorption capacities for a range of initial contamination varying between 15 $\mu\text{g/L}$ and 80 mg/L as reported in the literature [4,14,15]. However, alternatives are being sought to yield more cost-effective adsorbents. Biomass as an inexpensive but abundant material source for biosorption has been considered, yet the biosorbent non-regenerability and pollutant disposal is of a concern [4,16–18]. Over the past decade, nanomaterials have been tested for organic adsorption [19–21]. Their high surface to volume ratio reduces the required adsorbent dose and favours surface reactivity and therefore adsorption kinetics [19]. Nanofiber webs have been designed as a novel adsorptive material solution for water remediation, to benefit from the increased surface reactivity, with an easy handling and water-stable behaviour, as opposed to free nanotubes and nanoparticles, respectively [22]. Furthermore, electrospinning as a nanofiber web fabrication route ensures a high fiber diameter homogeneity and offers versatile web morphologies design [23].

This paper reviews the employment of nanofibers in the adsorption of selected organic pollutants. The first section is dedicated to common pesticides of moderate hydrophobicity, for water contamination levels over 1 mg/L . Selected pesticides are Alachlor, Atrazine, Chlorpyrifos and Diazinon. The second section concerns the adsorption of disinfectants such as phenol and selected chlorophenols, namely 2- and penta-. As phenol adsorption has been widely reported in the literature, phenol has been included in this study to benchmark the performance of nanofibers in the adsorption of phenolic compounds. Furthermore, this inclusion allows for the investigation of the impact of the molecule chlorine number onto the adsorbent uptake. The last section deals with persistent pollutants,

highly hydrophobic, including most of the POPs selected for this study. The pesticides reviewed in this section are aliphatic alicyclic organochlorines Aldrin, Dieldrin, Endrin, Chlordane, Heptachlor, Heptachlor epoxide, and Toxaphene 8. Other types of POP selected include polychlorinated biphenyls (PCBs) 2-, 3-, 4-, 5-, 6-, 28-, 77-. Polyaromatic hydrocarbon (PAH) Phenanthrene was also considered in this section for performance comparison.

Compared to other pesticide removal by adsorption reviews, the present paper gives exhaustive and up-to-date insight into the performance of nanofibers for the removal of several contaminants of different classes [4,24,25]. This study aims to help with the design of an efficient adsorbent for a targeted organic pollutant. Therefore, the influence of adsorbent physicochemical properties and adsorption conditions on the resulting performance was investigated in order to determine a specific range of adsorbent surface properties and advantageous test conditions to favour pollutant capture. Finally, a comparison of the adsorptive performance pondered by the proportion range order between adsorbent dose and initial contaminant concentration was made here to help with the design of a cost-efficient material solution.

Adsorbents' surface properties, performance and test conditions are reported in Section 2.3, Section 3.3 and Section 4.3 for the adsorption of moderately hydrophobic pollutants, phenolic compounds and highly hydrophobic pollutants, respectively. When either adsorption capacity or removal efficiency was not reported, it has been calculated from the reported performance result. When room temperature was reported, a temperature of 22 °C was chosen. Langmuir and Freundlich were considered among the isotherm models. Concerning kinetic models, pseudo first- and second-order, intra-particle diffusion and linear models were here reported.

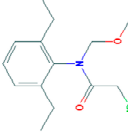
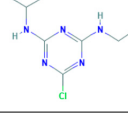
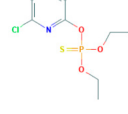
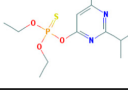
2. Moderately Hydrophobic Pesticides

In this section, the adsorptive performance of nanofiber-based adsorbents is reviewed and benchmarked against other reported adsorbents for Alachlor, Atrazine, Chlorpyrifos and Diazinon pesticides. After presenting the adsorbate molecules' characteristics, an analysis of the adsorbent structure-performance relationships will be given. First, the influence of adsorbent specific and contact surface area as well as pore volume will be reviewed. Then, the range order between adsorbent dose, initial concentration and obtained adsorption capacity will be highlighted.

2.1. Adsorbate Properties

Table 1 presents the molecular characteristics of the four pesticides considered in this section, namely Alachlor, Atrazine, Chlorpyrifos and Diazinon. Both Alachlor and Atrazine are organochlorine pesticides (OCPs). Alachlor is composed of an aniline aromatic structure, bound to an oxoacid and a chloroacetamide group via a central nitrogen group. Atrazine possesses a chlorotriazine aromatic structure, bound to two dimethylamine groups on the aromatic carbon atoms. Although Chlorpyrifos also possesses chlorine terminal groups, it is commonly classified with Diazinon as organophosphorus pesticides (OPPs). Chlorpyrifos aromatic structure is made of a ring of trichloropyridine, with attachment of the three chlorine groups on three of the ring's carbon atoms. To form Chlorpyrifos, the chloropyridine is bound to an organophosphate structure, composed of a modified phosphate group, which is double-bonded to a sulphur atom, also called phosphorothioate. Diazinon shares the same sulphur-phosphate structure, which is here bound to a pyrimidine or 1,3-diazine aromatic ring [26].

Table 1. Characteristics of Alachlor, Atrazine, Chlorpyrifos and Diazinon [26].

Name	Molecular		Log K _{ow}	Solubility in Water (mg/L, 25 °C)	2D Structure	H Bound Count	
	Weight (g/mol)	Formula				Donor	Acceptor
Alachlor	269.769	C ₁₄ H ₂₀ ClNO ₂	3.52	240		0	2
Atrazine	215.685	C ₈ H ₁₄ ClN ₅	2.61	34.7		5	2
Chlorpyrifos	350.575	C ₉ H ₁₁ Cl ₃ NO ₃ PS	4.96	1.4		5	0
Diazinon	304.345	C ₁₂ H ₂₁ N ₂ O ₃ PS	3.81	60		6	0

The reported molecular weights range from 216 g/mol for Atrazine up to 351 g/mol for Chlorpyrifos, with each of the pesticides carrying a different molecular configuration. In terms of molecular size, Atrazine followed by Alachlor are smaller than organophosphates Chlorpyrifos and Diazinon, which is of interest for the study of the molecule diffusion in an adsorbent material with reported pore features.

Hydrogen bond acceptor and donor counts are reported here to discuss the influence of chemisorption by H-bonding on the pesticide uptake by nanofiber adsorbents. Both Alachlor and Atrazine have an H-bond acceptor count of 2 due to their longer carbon chains. Atrazine, Chlorpyrifos and Diazinon have an H-bond donor count of 5, 5 and 6, respectively. H-bond donor groups are formed by amide and nitrogen groups in the case of Atrazine, and by nitrogen groups, as well as sulphur and oxygen atoms from the organophosphate backbone, as in the case of Chlorpyrifos and Diazinon. As each of the adsorbate molecules possesses an aromatic structure, adsorption by electron interaction through π - π stacking between the adsorbent surface unsaturated bonds and the molecule aromatic ring is believed to play a significant role in the pesticide uptake here [26,27].

Finally, the octanol-water partition coefficients are reported to point out the less hydrophobic character of the selected pesticides compared to persistent-classified pesticides, such as the here reviewed aliphatic organochlorines. Solubility in water at ambient temperature was also reported to give an insight into the maximum levels of water contamination achievable by these pesticides.

2.2. Nanofibers for Pesticide Adsorption

2.2.1. Impact of Adsorbent Specific and Contact Surface Area

Figure 1 shows the impact of the adsorbent specific surface area (BET) on the adsorption removal. The removal percentage was overall found to decrease with increasing adsorbent specific surface area for both Alachlor and Diazinon, yet was found to increase in the case of Atrazine removal.

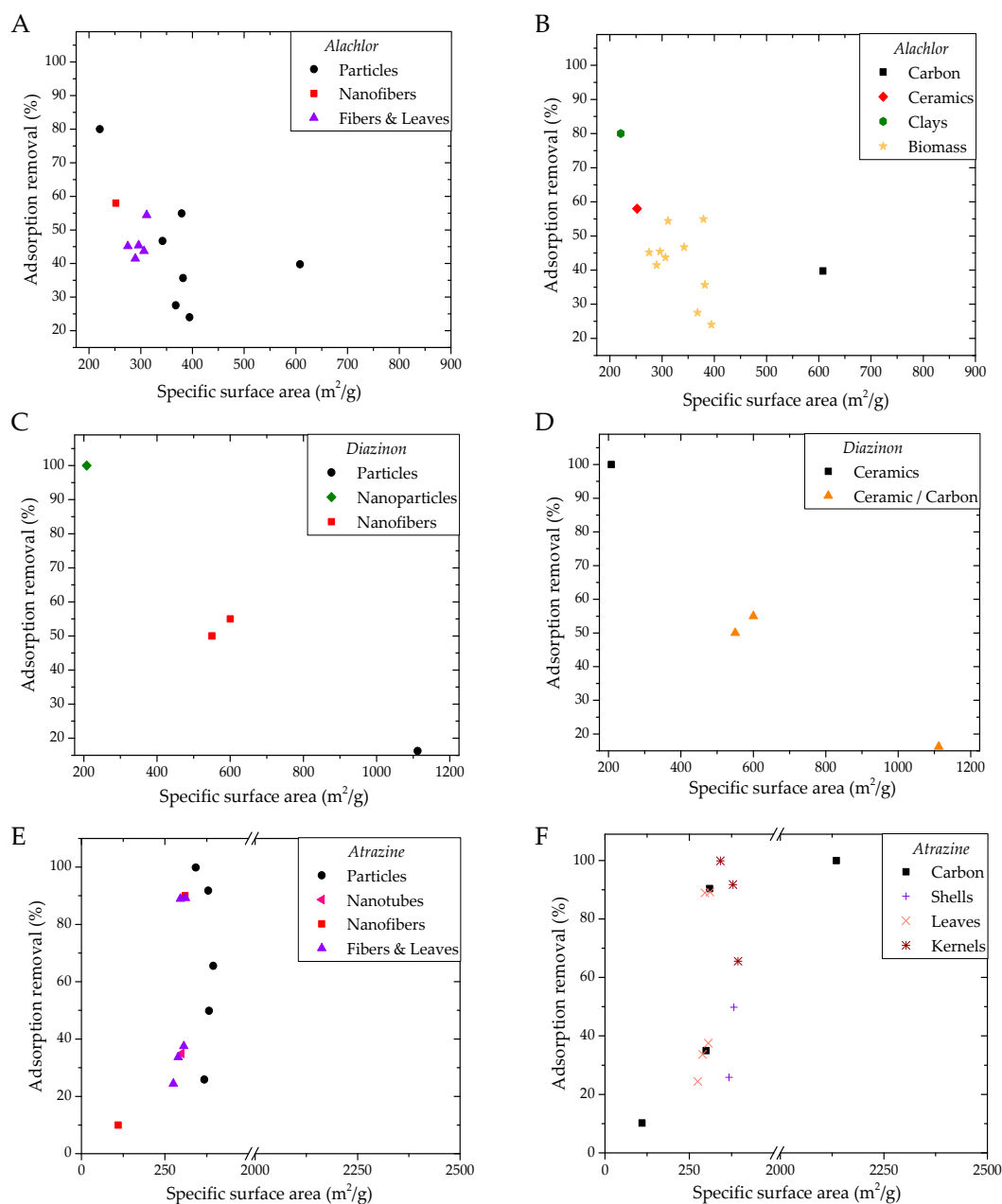


Figure 1. Adsorption removal (%) related to adsorbent specific surface area for different adsorptive structures and for different adsorbent compositions against Alachlor (A,B), Atrazine (C,D) and Diazinon (E,F).

Indeed, for Alachlor, as shown in Figure 1A, the maximum reported removal performance reached 80% for acid-activated beidellite clay particulates grafted with organosilanes for a BET of 221 m²/g (Table 2, N5). In comparison, the largest specific surface area of 608 m²/g of an activated charcoal adsorbent removed 40% of Alachlor (Table 2, N4). Nanofiber adsorbents made of alumina with surface-grafted organosilanes showed the second best performance with 58% removal for a specific surface area of 252 m²/g (Table 2, N1). The higher performance of organosilane-grafted clays and alumina nanofibers suggests that there is competition between adsorption via hydrophobic interactions and via electrostatic interactions as the most efficient mechanism for Alachlor uptake [28,29]. Indeed, organosilane grafting provides the adsorbent with a hydrophobic surface more amenable to pesticides [28]. Each adsorbent reported in this study for the adsorption of Alachlor differs in

both structure and composition. Figure 1B shows the different compositions of Alachlor adsorbents, revealing here a lower performance for carbon-based adsorbents (Table 2, N3) followed by biomass adsorbents made of kernels and leaves (Table 2, N6–N15). Several factors may explain the lower performance of activated charcoal, such as unsuitable surface pore characteristics not reported in the literature. A different structure than crystalline honeycomb carbon adsorbent may also impact the arrangement and coordination of adsorbate molecules on the charcoal surface, virtually decreasing the proportion in active sites compared to nitrogen adsorption, as well as discourage adsorption by electron interaction due to the absence of unsaturated bonds. Biomass adsorbents had a specific surface area between 275 and 394 m²/g, with vegetal-based adsorbents of a lower BET than kernel or stone-based adsorbents (Table 2, N13, N7). The lower BET and fibrous aspect of leaf material, allowing for a better diffusion of the pesticide, may contribute to the increased performance compared to kernel particulates.

A similar decreasing trend can be observed in the case of Diazinon removal in Figure 1C, although not enough data has been reported in the literature to accurately analyse the impact of adsorbent specific surface area on removal capacity. Adsorbents with lower specific surface areas such as 208 m²/g for iron oxide and silica nanocrystals were able to completely remove Diazinon, for an initial contamination of 400 µg/L and adsorbent dose of 6 g/L (Table 3, N4). The differences in levels of initial contamination and dose of adsorbents may impact the adsorptive performance comparison. Nanofiber adsorbents such as activated carbon nanofibers with manganese and alumina nanoparticles of a respective BET of 550 m²/g and 600 m²/g showed average removal around 55% (Table 3, N1, N2). The highest BET of the reported materials at 1112 m²/g for activated carbons led to the lowest adsorption performance amongst the series at 16.3% (Table 3, N6). Most of the adsorbent reported fitted the Langmuir isotherm model and the pseudo-second-order kinetic model well, which suggests a homogenous monolayer surface adsorption process that is rate-limited by chemisorption, and hence surface saturation [30]. Figure 1D presents different adsorbent compositions, showing the preferential adsorption of Diazinon on ceramic surfaces over ceramic–carbonaceous adsorbents.

Table 2. Nanofibrous adsorbent properties and adsorption conditions for the removal of Alachlor. BET: specific surface area.

N	Adsorbent	Adsorbent Properties			Adsorption Capacity (mg/g)	Adsorption Conditions						Removal (%)	Ref.	
		BET (m ² /g)	Pore Volume (cm ³ /g)	Pore Diameter (nm)		Initial P Concentration (µg/L)	Adsorbent Dose (g/L)	pH	Temperature (°C)	Eq. Time (h)	Kinetic Model			Isotherm Model
1	Organosilane-grafted alumina nanofibers	252	1	11.4	5.8	10,000	1		23	2.6			58	[28]
2	Organo/layered double hydroxide nanohybrids				113	94,000	0.67		25	2.5			80.5	[31]
3	Activated carbon	1110	0.7		90	100		5						[32]
4	Activated charcoal	608			0.16	40,000	100		35			Langmuir	39.7	[33]
5	Organosilane-grafted acid-activated beidellite clay	221	0.36	6.44	16	10,000	0.5		23	24			80	[29]
6	Bamboo canes	381			0.000018	0.5	10	6	40	7	Pseudo I order	Freundlich	35.7	[16]
7	Date stones	394			0.000012	0.5	10	6	40	7	Pseudo I order	Freundlich	24.0	[16]
8	Olive stones	379			0.000027	0.5	10	6	40	7	Pseudo I order	Freundlich	54.9	[16]
9	Peanut shells	368			0.000014	0.5	10	6	40	7	Pseudo I order	Freundlich	27.6	[16]
10	Avocado stones	342			0.000023	0.5	10	6	40	7	Pseudo I order	Freundlich	46.7	[16]
11	<i>Eucalyptus gomphocephala</i>	289			0.000021	0.5	10	6	40	7	Pseudo I order	Freundlich	41.5	[16]
12	<i>Raphanus raphanistrum</i>	296			0.000022	0.5	10	6	40	7	Pseudo I order	Freundlich	45.4	[16]
13	<i>Nerium oleander</i>	275			0.000022	0.5	10	6	40	7	Pseudo I order	Freundlich	45.2	[16]
14	<i>Origanum compactum</i>	306			0.000022	0.5	10	6	40	7	Pseudo I order	Freundlich	43.7	[16]
15	<i>Cistus ladaniferus</i>	311			0.000027	0.5	10	6	40	7	Pseudo I order	Freundlich	54.4	[16]

Table 3. Nanofibrous adsorbent properties and adsorption conditions for the removal of Diazinon.

N	Adsorbent	Adsorbent Properties			Adsorption Capacity (mg/g)	Adsorption Conditions						Removal (%)	Ref.	
		BET (m ² /g)	Pore Volume (cm ³ /g)	pH _{ZPC}		Initial P Concentration (µg/L)	Adsorbent Dose (g/L)	pH	Temperature (°C)	Eq. Time (h)	Kinetic Model			Isotherm Model
1	Activated carbon nanofibers with MgO nanoparticles	600	0.9		0.11	200	1			0.5			55	[34]
2	Activated carbon nanofibers with Al ₂ O ₃ nanoparticles	550	0.9		0.1	200	1			0.5			50	[34]
3	Sodalite zeolite coated with Cu ₂ O nanoparticles				29.15	50,000	0.3	6	20	2	Pseudo II order	Langmuir	97.2	[35]
4	Fe ₃ O ₄ /SiO ₂ nanocrystals	208		2.8	28	400	6	6	25	0.8	Pseudo II order	Langmuir	100	[36]
5	NH ₄ Cl modified activated carbon				97.5	20,000	0.3	7		0.5		Langmuir	97.5	[37]
6	Activated carbon modified with Fe particles	1112	0.663	4.01	65	40,000	0.1	6.5	25	2	Pseudo II order	Langmuir	16.3	[38]

Table 4. Nanofibrous adsorbent properties and adsorption conditions for the removal of Atrazine.

N	Adsorbent	Adsorbent Properties				Adsorption Capacity (mg/g)	Adsorption Conditions						Removal (%)	Ref.	
		BET (m ² /g)	Fiber Diameter (nm)	Pore Volume (cm ³ /g)	pH _{ZPC}		Initial P Concentration (µg/L)	Adsorbent Dose (g/L)	pH	Temperature (°C)	Eq. Time (h)	Kinetic Model			Isotherm Model
1	Carbon nanofibers	110	160	0.11		2.2	10,784	0.5	7		1			10.2	[39]
2	Polystyrene nanofibers					0.095	500	1					Lang.	19.0	[40]
3	Nylon/Polypyrrole core shell nanofibers					2.77	10,000	1	7	25	5	Pseudo II order	Freund.	27.7	[41]
4	Acid-modified polyacrylonitrile nanofibers		180			2.02	10,000	1		25	0.5			20.2	[41]
5	Polyacrylonitrile nanofibers		160			1.6	10,000	1		25	0.5			15.8	[41]
6	Carbon nanofiber/carbon nanotube composites	310	100	0.25		19.5	10,784	0.5	7		1			90.4	[39]
7	Carbon nanotubes	300	40	0.79	4.1	105	30,000	0.1	7.8	30	6		Lang.	35.0	[42]
8	Multi-walled carbon nanotubes	174	29	0.7	3.9	0.2	15	0.007					Freund.		[14]
9	Single-walled carbon nanotubes	406	2	1.11		130		1		25					[21]
10	Nano-graphene platelets	624	5000	2.69	9.5	1.99	15	0.007					Freund.	92.9	[14]
11	Superfine powdered activated carbon	773	240	1.01	5.7	1.78	15	0.007					Freund.	83.1	[14]
12	Powdered activated carbon	900	37,000	0.46	6.1	2.21	15	0.007					Freund.	99.9	[14]
13	Modified activated carbon	2135		0.919	6.6	62	30,000	0.5		25	4			99.9	[43]
14	Polyacrylic acid modified mesoporous carbon					25	15,000	0.5	5	30				83.3	[44]
15	Cellulose/graphene composites					0.32	1000	3	9	25	0.2		Lang.	96.0	[45]
16	Bamboo canes	381				0.000025	0.5	10	6	40	7	Pseudo I order	Freund.	49.8	[16]
17	Date stones	394				0.000033	0.5	10	6	40	7	Pseudo I order	Freund.	65.6	[16]
18	Olive stones	379				0.000046	0.5	10	6	40	7	Pseudo I order	Freund.	91.8	[16]
19	Peanut shells	368				0.000013	0.5	10	6	40	7	Pseudo I order	Freund.	25.9	[16]
20	Avocado stones	342				0.000050	0.5	10	6	40	7	Pseudo I order	Freund.	99.9	[16]
21	<i>Eucalyptus gomphocephala</i>	289				0.000017	0.5	10	6	40	7	Pseudo I order	Freund.	33.7	[16]
22	<i>Raphanus raphanistrum</i>	296				0.000044	0.5	10	6	40	7	Pseudo I order	Freund.	88.9	[16]
23	<i>Nerium oleander</i>	275.02				0.000012	0.5	10	6	40	7	Pseudo I order	Freund.	24.4	[16]
24	<i>Origanum compactum</i>	306.28				0.000018755	0.5	10	6	40	7	Pseudo I order	Freund.	37.5	[16]
25	<i>Cistus landaniferus</i>	311.42				0.000044605	0.5	10	6	40	7	Pseudo I order	Freund.	89.2	[16]

Concerning Atrazine removal, as represented in Figure 1E, the lower BET value reported at $110 \text{ m}^2/\text{g}$ for carbon nanofibers reached the least adsorption performance with a removal of 10.2% (Table 4, N1). Carbon nanotube–nanofiber composites and carbon nanotubes, however, reached a removal of 90.4% and 35% for a specific surface area of $310 \text{ m}^2/\text{g}$ and $300 \text{ m}^2/\text{g}$, respectively (Table 4, N6, N7). Higher specific surface areas of $2235 \text{ m}^2/\text{g}$ for activated carbons led to complete contaminant removal (Table 4, N13). As carbon-based materials are among the highest-performing adsorbents, this suggests that π – π electron interactions and electrostatic interactions are preferential adsorption mechanisms for the removal of Atrazine. Figure 1F shows the Atrazine adsorbents' composition and other carbon-based structures; biomass absorbance has been reported in this form or extracted from shells, kernels and leaves. For a similar range of specific surface area, kernel and shell adsorbents here showed better performance compared to their leaf counterparts, with over 99% and 89% highest removal percentages, respectively (Table 4, N20, N25). This difference in performance suggests that the adsorbent structure can significantly influence the Atrazine adsorption. Furthermore, all biomass adsorbents fitted the Freundlich isotherm and pseudo-first-order kinetic models well ($R^2 > 0.85$), suggesting a heterogeneously distributed adsorption on the biosorbent surface and physisorption as the reaction rate-limiting step [30]. This may suggest that Atrazine could not diffuse as much nitrogen into the adsorbent surface pores or between fibers' interstitial spaces.

The different trends of performance increase for Alachlor and Diazinon and decrease for Atrazine with increasing specific surface areas may be explained by the molecular geometry of the adsorbates and preferential adsorption mechanisms. Indeed, both Alachlor and Diazinon are planar molecules, while Atrazine is non-planar. Molecule planar geometry may favour the alignment of an adsorbate molecule onto an adsorptive site, while allowing other pesticide molecules to diffuse; a non-planar molecule when adsorbed might in a certain configuration form a blockage to other pesticide molecules. In such a scenario, a lower density of functional sites and consequently a lower specific surface area can result in improved adsorptive performance. Pesticide molecule polarity could also influence the localized adsorption on the adsorbent surface, limiting adsorption performance via hydrophobic interactions.

Figure 2 shows the variation in adsorption capacity related to the adsorbent diameter or sheet thickness, in the adsorption of Atrazine. An exponential-type decreasing trend of the adsorption capacity for increasing material size can be observed. Indeed, carbon nanotubes of 40 nm diameter demonstrated a capacity of 105 mg/g (Table 4, N7). On the other hand, granular activated carbon of $37 \mu\text{m}$ size showed a capacity below 10 mg/g (Table 4, N12). Carbon nanofibers and polyacrylonitrile nanofibers, both with a mean diameter of 160 nm, showed a capacity of 2.2 mg/g and 1.6 mg/g , respectively (Table 4, N1, N5). All adsorbents represented here are carbonaceous, and diameters below 200 nm were reported for nanomaterials adsorbents. A higher contact surface area, and hence a lower diameter, would thus increase the proportion of electron vacancies on the nano-adsorbent surface by decreasing the volume of bulk material. As carbon-based adsorbents are prone to adsorb by electron interaction, such as π – π stacking between adsorbent and adsorbate respective unsaturated bonds, more electron vacancies and hence a lower adsorbent diameter would result in improved performance. The choice of adsorbent structure does not seem to impact on the performance, suggesting that the surface chemistry and charge distribution play a major role in the adsorptive performance. In this study, adsorbent diameters below 100 nm on average led to adsorption capacities over 20 mg/g for the removal of Atrazine.

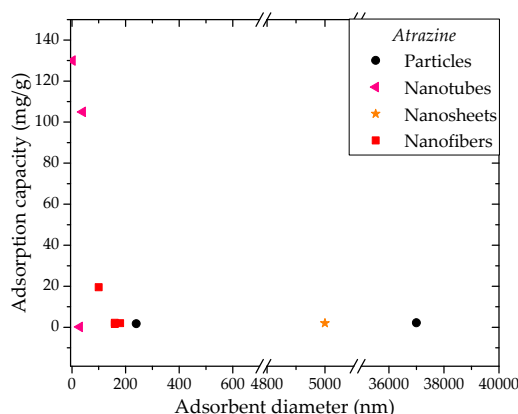


Figure 2. Adsorption capacity (mg/g) related to the adsorbent diameter against Atrazine.

2.2.2. Impact of Adsorbent Pore Size and Pore Volume

Figure 3 shows adsorption capacity related to the adsorbent pore volume in the removal of Atrazine. A global trend of increasing capacity for an increased pore volume up to $1.1 \text{ cm}^3/\text{g}$ can be noticed (Table 4, N9). This overall trend may be explained by the higher number of atrazine molecules diffusing in a higher number of surface pores across larger pore channels. However, several factors can imply lower performance for a higher pore volume. Adsorbent surface pore size is a critical factor for pesticide diffusion. For instance, surface pores twice as large as the adsorbate molecule cross section could still allow pesticide diffusion if one molecule was adsorbed along one pore wall, and could even allow two molecules to adsorb side to side. Yet, a larger pore channel would not favour the adsorption along pore walls due to a lower promiscuity. Furthermore, a higher pore volume could also translate to a higher proportion of pores with a smaller size distribution falling below the pesticide molecule size or cross section, hence hindering the adsorbate diffusion. Also, dead-end pores would affect the determination of pore volume. Nevertheless, the overall trend indicates that a pore volume around $1.0 \pm 0.1 \text{ cm}^3/\text{g}$ is preferential for increased performance in the removal of Atrazine.

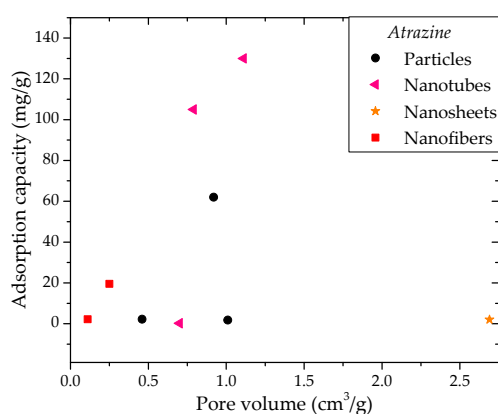


Figure 3. Adsorption capacity (mg/g) related to the adsorbent pore volume against Atrazine.

Concerning the adsorbent pore size, not enough data were found in the literature to enable a study of a preferential pore diameter for a specific pollutant among the ones considered in this section. In the case of Alachlor adsorption, organosilane-grafted beidellite clay and alumina nanofibers were reported to have a pore diameter of 6.44 nm and 11.4 nm, respectively, and showed an efficiency of 80% and 58% (Table 2, N1, N5) [28,29]. These results may suggest that an 11.4 nm wide pore channel does not offer enough promiscuity for the adsorption of Alachlor molecules, combined with a possible decrease in the efficiency of silane grafting along the adsorbent pore walls, thus impeding adsorption

via hydrophobic interactions. Indeed, organosilane compounds considered for alumina nanofiber grafting include CPTES (3-chloro-propyl-triethoxysilane) and OTES (octyl-triethoxysilane), both of a weight comparable to Alachlor, 241 g/mol and 277 g/mol, of single-molecule orientation and longer carbon chain.

2.2.3. Nanofiber Performance Comparison Regarding Initial Pesticide Concentration and Adsorbent Dose

Figure 4 shows bar charts representing the adsorption capacity with the corresponding tests conditions of initial pesticide concentration and adsorbent dose for each pesticide, nanofiber adsorbent and selected benchmark adsorbents. It can be noticed from all the charts that nanofibers delivered an adsorption performance on average in the range of other benchmarked adsorbents. Indeed, nanofiber adsorption capacities ranged from 5.8 to 19.5 mg/g (Table 2, N1 and Table 4, N6), for a similar range of initial dye concentration around 10 mg/L compared to benchmark materials, yet for an adsorbent dose on average below 1 g/L. Other macro-adsorbents were reported for a dose on average over 3 g/L. The lower adsorbent dose required for nano-adsorbents compared to macrostructures should be taken into consideration when calculating the material fabrication cost and regeneration volumes.

In the case of organochlorines, Organo-layered double hydroxide nanohybrids and single walled carbon nanotubes showed the highest adsorption capacities of 113 mg/g and 130 mg/g against Alachlor and Atrazine, respectively (Table 2, N2 and Table 4, N9). However, other ceramic and carbon adsorptive nanostructures showed a lower performance for the same adsorbate respectively. Indeed, organosilane/alumina nanofibers demonstrated a capacity of 5.8 mg/g against Alachlor (Table 2, N1), and carbon nanofiber/carbon nanotube composites showed a capacity of 19.5 mg/g against Atrazine (Table 4, N6). Other than the action of other adsorption mechanisms, these performance differences for similar adsorbent sizes and compositions may also be explained by a different adsorbent pore structure that is hindering the diffusion of the pesticides, as in the case of modified alumina nanofibers, for example. Nevertheless, the predominant efficiency of carbon and metal oxide adsorbent surfaces suggests that π - π electron and electrostatic interactions are the most efficient adsorption mechanisms towards selected pesticides, compared to hydrophobic interactions, which by comparison reached average performance when serving as the predominant mechanism at stake [29]. Furthermore, carbon nanofibers were reported to show adsorptive affinity for other contaminants, such as sulfamethoxazole, in a multi-contaminant flow through adsorption test, demonstrating the versatility of carbonaceous adsorbents towards organic molecules with unsaturated bonds such as aromatic rings [39]. Polystyrene molecular imprinted nanofibers showed limited performance against Atrazine and Chlorpyrifos (Table 4, N2 and Table 5, N1). Although polyester is a hydrophobic polymer and is thus supposed to show affinity to the pesticides studied here, it is suggested that adsorption may be limited by an unsuitable solution pH, conferring on both adsorbent and adsorbate a similar surface charge [40]. Nylon-Poly(pyrrole) core-shell nanofibers showed an adsorption capacity of 2.77 mg/g, corresponding to an efficiency of 27% (Table 4, N3). The aromatic ring of Poly(pyrrole) enables π - π interaction with the Atrazine triazine ring, while nylon does not have unsaturated bonds [41]. Experiments here were reported for a neutral solution pH. However, the Poly(pyrrole) isoelectric point has been reported around 10, meaning that at neutral pH both adsorbent and atrazine exhibited a positive surface charge [41]. It was concluded that a pH slightly above 10 would favour adsorption with a negative Poly(pyrrole) surface and still slightly protonated atrazine [41].

In the case of organophosphates, benchmark adsorbents tested in similar conditions to nanofiber adsorbents could rarely be found. For instance, activated carbon nanofibers modified with either magnesium or aluminium oxide nanoparticles showed a capacity of 0.1 mg/g against Diazinon (Table 3, N1, N2). Still, against Diazinon, granular activated carbon (GAC) modified with iron oxide particles reached a capacity of 65 mg/g (Table 3, N6). Although iron oxide would be more reactive than magnesium or aluminium oxides, the large difference in applied adsorbent dose (1g/L for nanofibers and 0.1 g/L for GAC) and in initial concentration (200 μ g/L for nanofibers and 40 mg/L for GAC)

would significantly impact on the difference in performance. This influence stems from the equation used to determine the adsorption capacity. Adsorptive studies carried out on adsorbent dose and level of contamination in similar conditions to those reported for the polystyrene nanofiber study could not be found in the literature (Table 5, N1).

It can be noticed from Figure 4 that higher adsorbent doses, above 5 g/L, result on average in poorer adsorption capacities, falling below 1 mg/g (Table 2, N4). Similarly, for an average adsorbent dose around 1 g/L, a lower initial dye concentration below 0.5 mg/L tends to result in a lower adsorption capacity (Table 4, N2). These tendencies can be explained by the theory used to calculate the adsorption capacity, which will be reduced for higher adsorbent doses or lower initial dye concentrations, yet have the same removal efficiency. The optimal adsorbent dose required for a given initial concentration and a target removal efficiency could be more consistently investigated among the adsorptive studies to enable a rigorous performance comparison.

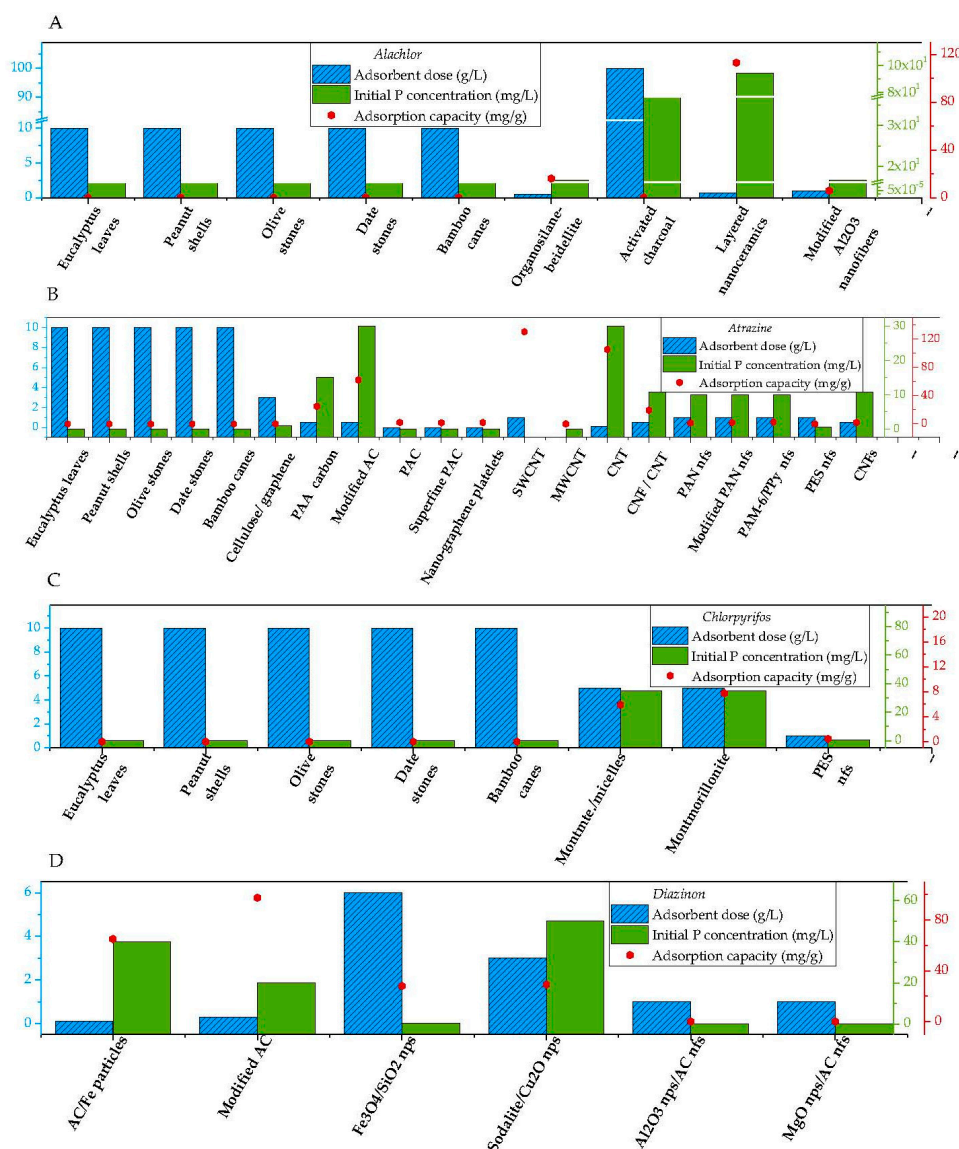


Figure 4. Relation between adsorbent dose (blue column, left scale), initial pesticide concentration (green column, middle right scale) and adsorption capacity (red scatter, far left scale) in the adsorption of Alachlor (A); Atrazine (B); Chlorpyrifos (C) and Diazinon (D).

Table 5. Nanofibrous adsorbent properties and adsorption conditions for the removal of Chlorpyrifos.

N	Adsorbent	Adsorbent Properties	Adsorption Capacity (µg/g)	Adsorption Conditions							Removal (%)	Ref.	
		BET (m ² /g)		Initial P Concentration (µg/L)	Adsorbent Dose (g/L)	pH	Temperature (°C)	Eq. Time (h)	Kinetic Model	Isotherm Model			
1	Polystyrene nanofibers		450	500	1						Langmuir	90	[40]
2	Modified montmorillonite		7760	35,000	5		35				Freundlich	100	[46]
3	Montmorillonite-micelles composite		5910	35,000	5		20				Freundlich	84.4	[46]
4	Bamboo canes	382	0.032	0.5	10	6	40	7	Pseudo I order	Freundlich		63.3	[16]
5	Date stones	394	0.036	0.5	10	6	40	7	Pseudo I order	Freundlich		71.63	[16]
6	Olive stones	379	0.047	0.5	10	6	40	7	Pseudo I order	Freundlich		93.71	[16]
7	Peanut shells	368	0.030	0.5	10	6	40	7	Pseudo I order	Freundlich		60.1	[16]
8	Avocado stones	342	0.049	0.5	10	6	40	7	Pseudo I order	Freundlich		97.4	[16]
9	<i>Eucalyptus gomphocephala</i>	289	0.040	0.5	10	6	40	7	Pseudo I order	Freundlich		79.94	[16]
10	<i>Raphanus raphanistrum</i>	296	0.044	0.5	10	6	40	7	Pseudo I order	Freundlich		88.36	[16]
11	<i>Nerium oleander</i>	275	0.043	0.5	10	6	40	7	Pseudo I order	Freundlich		85.74	[16]
12	<i>Origanum compactum</i>	306	0.036	0.5	10	6	40	7	Pseudo I order	Freundlich		71.89	[16]
13	<i>Cistus landaniferus</i>	311	0.032	0.5	10	6	40	7	Pseudo I order	Freundlich		64.49	[16]

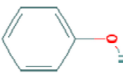
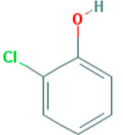
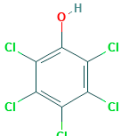
3. Phenolic Compounds

This section reviews the performance of nanofibers reported in the adsorption of phenol, 2- and penta-chlorophenol. Other than adsorptive performance relationships with adsorbent specific surface area and pore characteristics, the influence of the adsorbate chlorine number on adsorption will be investigated. Finally, test conditions such as pH, initial contamination and adsorbent dose will be taken into consideration.

3.1. Adsorbate Properties

Table 6 presents the molecular characteristics of Phenol, 2-Chlorophenol and Pentachlorophenol. Phenol, or carboic acid, is a base molecule for phenolic compounds, such as explosive nitrophenols or persistent pentachlorophenol. All three compounds considered in this study have been used as disinfectants. The phenol molecule is composed of an aromatic ring derived from benzene and bound to one hydroxyl group. Phenol's smallest cross section has been calculated at 0.43 nm. The 2-chlorophenol molecule is derived from phenol, with one chlorine group attachment on the aromatic ring, at position 2. Pentachlorophenol possesses five chlorine attachments to the aromatic ring, the sixth being the hydroxyl group, a component of the phenol molecule [26]. All three molecules possess three unsaturated bonds, conferred by the benzene-like aromatic structure, thus favouring adsorption via electron π - π stacking, provided on the adsorbent surface chemistry.

Table 6. Characteristics of Phenol, 2-Chlorophenol, and Pentachlorophenol [26].

Name	Molecular		Log K_{ow}	Solubility in Water (mg/L, 25 °C)	2D Structure
	Weight (g/mol)	Formula			
Phenol	94.113	C ₆ H ₆ O	1.46	67	
2-Chlorophenol	128.555	C ₆ H ₄ ClOH	2.15	28	
Pentachlorophenol	266.323	C ₆ HCl ₅ OH	5.12	14	

The number of chlorine groups influences not only the molecular weight but also molecule water solubility, decreasing from 67 to 14 mg/L for phenol and pentachlorophenol, respectively (25 °C). A decrease in water solubility results in an increase in the octanol-water partition coefficient. The higher chlorine number is also believed to promote the action of hydrophobic interactions on the capture of chlorophenol molecules, providing more surface area to react with a hydrophobic adsorbent. Finally, these three molecules possess a hydroxyl termination group as part of the phenol molecule, meaning each molecule possesses one hydrogen bond donor or acceptor group [26]. As a consequence, electrostatic interactions between the adsorbent surface and the contaminant hydroxyl group could also influence the adsorbent adsorption performance.

3.2. Nanofibers for Disinfectant Adsorption

3.2.1. Impact of Adsorbent Specific and Contact Surface Area

Figure 5 shows the adsorption performance of phenol and chlorophenols related to the adsorbent specific surface area. A near-linear trend of increase in the adsorption capacity for increasing adsorbent

specific surface area can be observed in the case of phenol adsorption, as shown in Figure 5A. This near-linearity can be bound to a near-homogeneous surface saturation process, with a higher proportion in adsorptive sites, i.e., BET proportionally corresponding to a higher adsorption capacity. In over 80% of the reported kinetic and isotherm studies for phenol adsorption, adsorbents were found to follow pseudo-second order and Langmuir models, translating into a surface monolayer adsorption reaction that is limited by chemisorption, hence further suggesting homogeneous surface saturation (Table 7). Plain carbon nanofibers and iron-oxide-decorated carbon nanofibers demonstrated a capacity of 0.842 and 1.684 mg/g for a specific surface area of 40.7 and 72.4 m²/g, respectively (Table 7, N17, N18). However, activated carbon nanofibers showed a higher performance of 256.1 mg/g for a higher BET of 2921 m²/g (Table 7, N20). Figure 5B details the adsorbent composition used for phenol capture, showing a majority of carbon or carbon-based adsorbents following the near-linear adsorption trend. An explanation of this adsorption performance trend formed by carbonaceous adsorbents relies on the donor–acceptor electron complex adsorption mechanism. Actors in the electron interaction for adsorption are the carbonyl groups on the carbon-adsorbent surface (electron donor), the proportion of which influences the specific surface area, and the phenol compound aromatic ring (electron acceptor) [4].

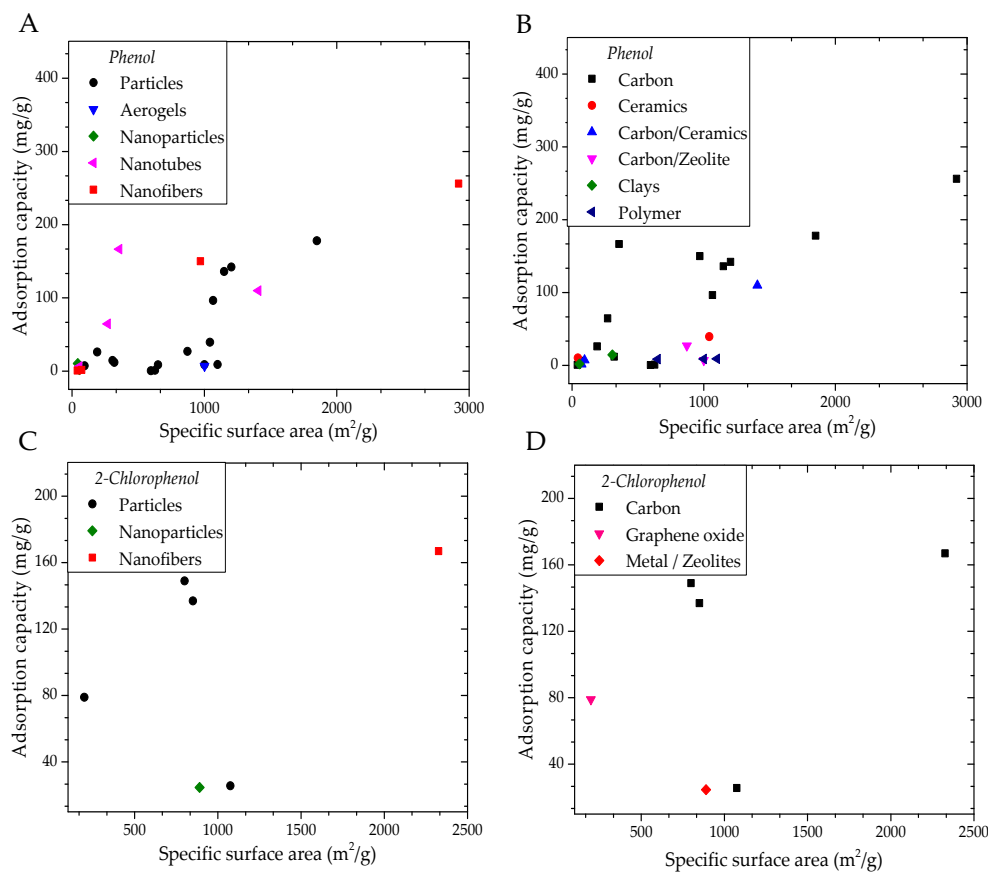


Figure 5. Cont.

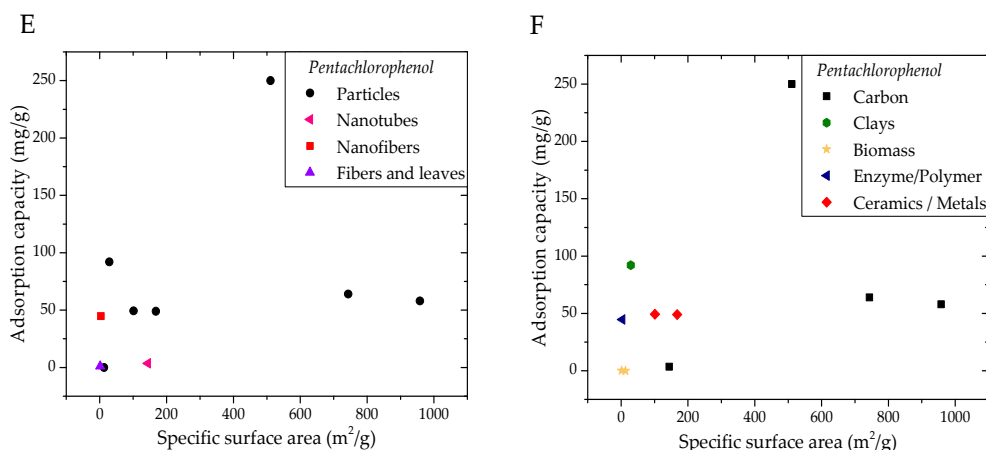


Figure 5. Adsorption capacity related to adsorbent specific surface area for different adsorptive structures and different adsorbent compositions against Phenol (A,B); 2-Chlorophenol (C,D) and Pentachlorophenol (E,F).

The observed preference for the Langmuir isotherm model can further be linked to the role of π - π dispersion forces between the aromatic rings of phenol and activated carbon. Indeed, a process of localized monolayer adsorption could signify that each site is accommodating a single molecule with repulsive interactions between adsorbed molecules [4]. Ceramic and clay adsorbents, although less reported, also showed to follow the adsorption trend. Therefore, adsorbent structure rather than composition is affecting the performance for a given BET. Styrene divinylbenzene particles, here reported under polymer adsorbents and not following the trend, have a particle size in the macro-range, and offered a capacity of 8.83 mg/g for a BET of 1000 m²/g (Table 7, N32). In the case of carbon nanotubes, which do not fit the global performance trend, their capacity of 166.58 mg/g for a BET of 357 m²/g (Table 7, N25) may be explained by their hollow structure. Variations in test conditions may also significantly affect the adsorbent performance for a given specific surface area. For instance, temperature was shown to act as a catalyst for phenol adsorption on doped cryptomelane manganese nanofibers, with faster metal oxide surface hydroxylation reported for temperatures from 140 °C (Table 7, N19). The created surface hydroxyl groups can bind to phenol and form phenolic complexes, thus enhancing the adsorption capacity even for a relatively low specific surface area of 40 m²/g, impeded by the higher density of metals compared to carbon atoms [47].

On the other hand, no clear trend can be pulled out in the case of 2- and pentachlorophenol adsorption, presented in Figure 5C–F respectively. Although fewer data are available, it can be seen that the higher the chlorine number on the adsorbate, the smaller the range of obtained adsorption capacities. Carbon nanofibers with a BET of 2326 m²/g showed the maximum capacity of 167 mg/g for 2-chlorophenol adsorption (Table 8, N1). In the case of pentachlorophenol, carbon black with a specific surface area of 511 m²/g was reported to show a capacity of 250 mg/g (Table 9, N6). However, over 90% of the adsorbents showed a capacity between 44.7 and 98 mg/g for a BET ranging from 3.7 to 958 m²/g for the capture of pentachlorophenol (Table 9, N1, N5, N12). The gradual decrease in observed performance for an increasing number of chlorine groups on the phenol molecule can be explained by the larger structure and the modified surface polarity of the molecule. Indeed, the chlorine group, being an electron-withdrawing group, lowers the aromatic ring electron density, or deactivates the ring, thus potentially hindering adsorption onto carbon or metal oxide surfaces by electron interaction and hindering hydrophobic interactions.

Table 7. Nanofibrous adsorbent properties and adsorption conditions for the removal of Phenol.

N	Adsorbent	Adsorbent Properties				Adsorption Capacity (mg/g)	Adsorption Conditions							Ref.
		BET (m ² /g)	Fiber Diameter (nm)	Pore Volume (cm ³ /g)	Pore Diameter (nm)		Initial P Concentration (mg/L)	Adsorbent Dose (g/L)	pH	Temperature (°C)	Eq. Time (h)	Kinetic Model	IsoT. Model	
1	Commercial Activated Carbon	596				0.57	30		6.8	20	6	Pseudo II order	Freund.	[48]
2	Activated carbon extracted from agro-waste (<i>Hemidesmus indicus</i>)	627				1.04	30		6.8	20	5	Pseudo II order	Freund.	[48]
4	Activated carbon extracted from tea industrial waste	1066		0.58	2.18	96.5	400	2	6		4	Pseudo II order	Lang.	[49]
6	Activated carbon extracted from Miswak root treated with KMnO ₄	1204				142.15	100	1	5	30	2		Freund.	[50]
7	Activated carbon produced from sludge	319.5			4	12	100	6	5.5	25	8	Pseudo II order	Freund.	[51]
8	Iron modified granular activated carbon	95		0.083		7.2	50	10	6.5	30	4	Pseudo I order	Lang.	[52]
9	Ammonia-treated coal reject	190			0.78	26.1	240	5	6	25				[53]
10	Powdered activated carbon	1149		0.644		136	200			30				[54]
11	Zeolite X/activated carbon composites	872		0.59		27.06	240	6	6.5	25	5	Pseudo II order		[55]
12	PET-based activated carbons	1850		0.743	0.8	178	150	5		24	1	Pseudo II order	Lang.	[56]
13	Ammonia-treated activated carbon microfibers					275	100	0.6		38	0.5		Freund.	[57]
14	Sawdust					5.5	100	10	5.8	22	3			[58]
15	Porous clay	305.5			3.7	14.5	450	8	5.5	25			Lang.	[59]
16	Activated carbon microfibers/carbon nanofibers composite	970		0.537		150	100	0.6		38	0.5		Freund.	[57]
17	Carbon nanofibers decorated with ferric oxide nanoparticles	72.4				1.684	2		7				Lang.	[60]
18	Carbon nanofibers	40.7				0.842	2		7				Lang.	[60]
19	Doped hydrophobic Cryptomelane type manganese oxide nanofibers	40		0.19		2060	5000	1		25	2			[47]
20	Activated carbon nanofibers	2921		2.7	0.43	256.1	300	0.5		38	1.3	Pseudo II order	Freund.	[61]
21	Hydroxyapatite nanopowders	43.75				10.33	400	1	6.4	60	2	Pseudo II order	Freund.	[62]
22	Ni/Cu MOF composites	1042.1		0.6241		39.47	50	1	5	30				[63]
23	Magnetic and cationic surfactant diatomite nanocomposite	55.7			15	2	10	0.5					Lang.	[64]
24	NiFe ₂ O ₄ nanoparticles aggregated on powdered activated carbon					33	200	0.6	8	25	5	Pseudo II order	Lang.	[65]
25	Carbon nanotubes	357		0.142		166.58	500	2.5		23	96		Freund.	[66]
26	Chitosan/Carbon nanocomposite particles					409	800	5		30	1	Pseudo II order	Freund.	[67]

Table 7. Cont.

N	Adsorbent	Adsorbent Properties				Adsorption Capacity (mg/g)	Adsorption Conditions							Ref.	
		BET (m ² /g)	Fiber Diameter (nm)	Pore Volume (cm ³ /g)	Pore Diameter (nm)		Initial P Concentration (mg/L)	Adsorbent Dose (g/L)	pH	Temperature (°C)	Eq. Time (h)	Kinetic Model	IsoT. Model		
27	Carbon nanotubes/MIL-68 (Al) composites	1407				109.9	500	1		30					[68]
28	Multi-walled carbon nanotubes	270				64.6	50	2	4.65		1	Pseudo II order	Freund.		[69]
29	Ethanol and heat treated carbon nanotubes	55.4		0.18		6.39	50	0.5		25					[70]
30	3D graphene aerogels—mesoporous silica frameworks	1000.8		0.93	1.87	6.95	4.4	2		25	2	Pseudo II order	Freund.		[71]
31	Commercial Styrene divinylbenzene particles—Dowex Optipore L493	1100			4.6	8.97	38	10		25	1	Pseudo II order	Freund.		[72]
32	Commercial Styrene divinylbenzene particles—Diaion SP825	1000			12	8.83	38	10		25	5	Pseudo II order	Freund.		[72]
33	Commercial Brominated styrene divinylbenzene particles—Diaion SP207	650			10.5	8.63	38	10		25	5	Pseudo II order	Freund.		[72]

Table 8. Nanofibrous adsorbent properties and adsorption conditions for the removal of 2-chlorophenol.

N	Adsorbent	Adsorbent Properties				Adsorption Capacity (mg/g)	Adsorption Conditions							Ref.	
		BET (m ² /g)	Fiber Diameter (nm)	Pore Volume (cm ³ /g)	pH _{ZPC}		Initial P Concentration (mg/L)	Adsorbent Dose (g/L)	pH	Temperature (°C)	Eq. Time (h)	Kinetic Model	Isotherm Model		Removal (%)
1	Carbon nanofibers	2326	500	1.36	4.4	167	10	0.05	6.5	25	5			84	[73]
2	Powdered activated carbon	800		0.8		149	200	1		25				75	[74]
3	Granular activated carbon	850		1.19		137	200	1		25				69	[74]
4	Powdered activated carbon	1075		0.78	2.8	25.7	10	0.05	6.5	25	5			13	[73]
5	Zeolite					46.1	65	1	9.3	25	2	Pseudo II order		71	[75]
6	Modified graphene oxide	198				79	50	0.6	5.5	25			Freund.	97	[76]
7	Cu-nano zeolite	890		0.18		24.7	50	0.6	6		2.5	Pseudo II order	Freund.	95	[77]

Table 9. Nanofibrous adsorbent properties and adsorption conditions for the removal of Pentachlorophenol.

N	Adsorbent	Adsorbent Properties			Adsorption Capacity (mg/g)	Adsorption Conditions							Ref.	
		BET (m ² /g)	Pore Volume (cm ³ /g)	Pore Diameter (nm)		Initial P Concentration (µg/L)	Adsorbent Dose (g/L)	pH	Temperature (°C)	Eq. Time (h)	Kinetic Model	Isotherm Model		Removal (%)
1	Encapsulated horseradish peroxidase in PEO-PPO nanofibers	3.73			44.7	10,000	0.5	3	25		Pseudo II order		83	[78]
2	Activated carbon fiber				175	300,000	0.5	12	25		Intra. diffusion	Langmuir	29.2	[79]
3	H ₂ O ₂ -oxidised multi walled carbon nanotubes	144			3.5	1200	0.2		35				58.2	[80]
4	Magnetic powdered activated carbon	743.6			64	80,000	1	5.75	20	1	Pseudo II order	Langmuir	80.0	[15]
5	Powdered activated carbon	958			58	80,000	1	5.75	20	1	Pseudo II order	Langmuir	72.5	[15]
6	Carbon black	511	1.42		250	700,000		7	20			Langmuir		[81]
7	Zero valent iron ZVI magnetic biochar composites	101	0.079	4.78	49.3	10,000	0.2	7		8			84	[82]
8	Ni-ZVI magnetic biochar composites	168	0.087	2.32	49	10,000	0.2	6	25	1	Pseudo I order		98	[83]
9	Hexagonal mesoporous silicas HMS	755	0.84	3.2		190		6	25			Freundlich	4	[84]
10	Aminopropyl-modified HMS	706	0.4	3.6		190		6	25			Freundlich	25	[84]
11	Hydrophobically modified thermo sensitive hydrogels				2.3	2663	1.67	3	25	5	Pseudo II order	Langmuir	95	[85]
12	Bentonite	29	0.072	3.81	92	300,000	5		25			Langmuir	100	[86]
13	Almond shell residue	13			0.005	100	10		30	24			93	[87]
14	Fungal biomass	1.4			0.094	1000	10	5	20	2	Pseudo II order	Langmuir	94	[88]

3.2.2. Impact of Adsorbent Pore Size

The impact of adsorbent pore size on the adsorption capacity against phenol is illustrated on Figure 6. There is a noticeable trend, characterised by an exponential-type decrease in the adsorption capacity with the increase of adsorbent pore size.

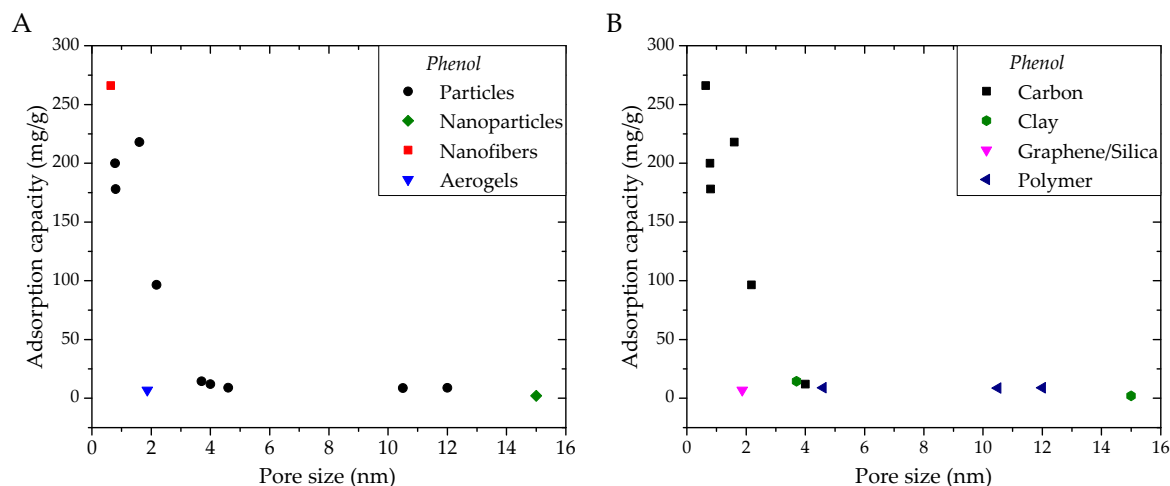


Figure 6. Phenol adsorption capacity related to the pore size of different adsorbent structures (A) and compositions (B).

For phenol capture, adsorbent pore size was reported from 0.43 nm (activated carbon nanofibers, Table 7, N20) to 15 nm (diatomite nanocomposites, Table 7, N23), corresponding to an adsorption capacity of 256.1 and 2 mg/g, respectively, being the maximal and minimal capacities here reported. Maximum adsorption capacities were observed for a pore size in a range between 0.43 and 2.2 nm (Table 7, N20, N4). The optimum pore size range of the adsorbent can be linked to the kinetics of pore blocking (i.e., phenol diffusion rate), adsorbent pore geometry and the single orientation of the phenol molecule (Table 6). Considering that the smallest cross section of the phenol molecule is 0.43 nm, mesopores (from 2 to 50 nm) may insufficiently promote adsorbent/adsorbate contact, thus resulting in a potentially lower performance depending on the adsorption mechanisms at stake (Table 7, N7, N32). On the other hand, activated carbon nanofibers were shown to possess an open pore structure and a dual pore size repartition of 0.43 nm and 0.8 nm, allowing the penetration of one or two phenol molecules, respectively (Table 7, N20). Dual pore size distribution on adsorbent surfaces can be further advocated by the fitting of the adsorption reaction to a Freundlich isotherm.

Furthermore, average adsorbent pore size has been calculated from a Barrett-Joyner-Halenda (BJH) method, and may not accurately reflect the adsorbent pore size distribution, depending on the actual pore tortuosity. However, a pore size calculated by BJH method and falling in the optimal range defined above may suggest an increased volume of micropores enhancing phenol adsorption. Using a BET/BJH method, the presence of micropores leads to an isotherm of type I, with increased nitrogen adsorption at low pressures [53]. Similarly to a Langmuir isotherm, the height of the plateau on the isotherm would reflect the volume of micropores, also called micropore capacity at the adsorbent surface. The extension of the isotherm hysteresis to relatively low pressures would give an indication of the micropores' diameter [53].

Beside the adsorbent morphology, voids between the nanofibers in the case of fibrous mats could also impact the diffusion of the phenol molecules; however, over 95% of the studies reported a nanofiber web fabrication by a solution blowing or electrospinning process, hence ensuring webs of high porosity and of suitably large pore sizes to enable phenol diffusion. This last aspect is critical as the hydrodynamics of the solution diffusion, and therefore the impact of the webs' wettability, is critical to the design of nanofibrous adsorbents.

3.2.3. Impact of Adsorbent Surface Charge and Solution pH

Adsorbent isoelectric point (IEP) corresponds to the pH at which the adsorbent carries no net electrical charge and is used to determine adsorbent global surface charge in an aqueous medium in function of the solution pH. As phenol and phenolic compounds are polar molecules, the adsorbent surface charge can significantly enhance the phenolic compound adsorptive performance with the attraction of two opposite charges between adsorbent and adsorbate. Phenol adsorption up to pH 7 has been experimented on with carbon nanofibers, resulting in a 31% removal capacity [89]. Nevertheless, the adsorbent IEP was not reported. Considering that phenol is a weak acid with a pKa of 9.95 (Table 6), an iso-electric point between pH 4 and pH 6.5 would be ideal to get the phenol molecule to bind to a carbon adsorbent surface for a reaction pH slightly below the adsorbent theoretical IEP and the phenol pKa. Adsorption studies at a reaction pH superior to the adsorbate pKa have been carried out for meta-aramid/polyacrylic acid nanofibers on another phenol compound, namely 2,4-dichlorophenol [90]. It was reported that the phenol compound dissociated into chlorophenolate anions, thus impeding the adsorption performance, given the electrostatic repulsion between identical charged target molecules and fiber active sites [90]. Solution pH therefore plays a determinant role in the efficiency of adsorption by electrostatic interaction. Ionic strength also has an impact on the adsorption process. Indeed, electrical double layers can form on the adsorbent surface [41]. In a case of a neutral pH, when falling below the adsorbent isoelectric point the adsorbent surface would carry a positive charge, and would therefore attract the anions present in the solution to the interface to form what is called a stern layer. The protonated contaminant would also carry a positive surface charge and would be found in the diffuse layer, attracted by anions in the stern layer. The thickness of the electrical double layers can prevent the adsorption reaction. However, when the ionic strength increases, the electrolyte will compress the electrical double layer and thus influence electrostatic interactions between adsorbate and adsorbent [41].

Figure 7 shows the variation in adsorption performance in function of the solution pH. It can be seen from all graphs that, starting from a solution pH of 6, the performance decreases with increasing pH. A solution pH between 4.5 and 6 seems to be the optimal window for metal oxide- and carbon-based adsorbents, confirming the theory explained above. The microfiber/nanofiber carbon composite adsorbent was surface-functionalized with ammonia [57]. It was reported that the inclusion of nitrogen groups on the adsorbent surface increased the adsorbent basicity, thus facilitating phenol adsorption at a close to neutral pH [57].

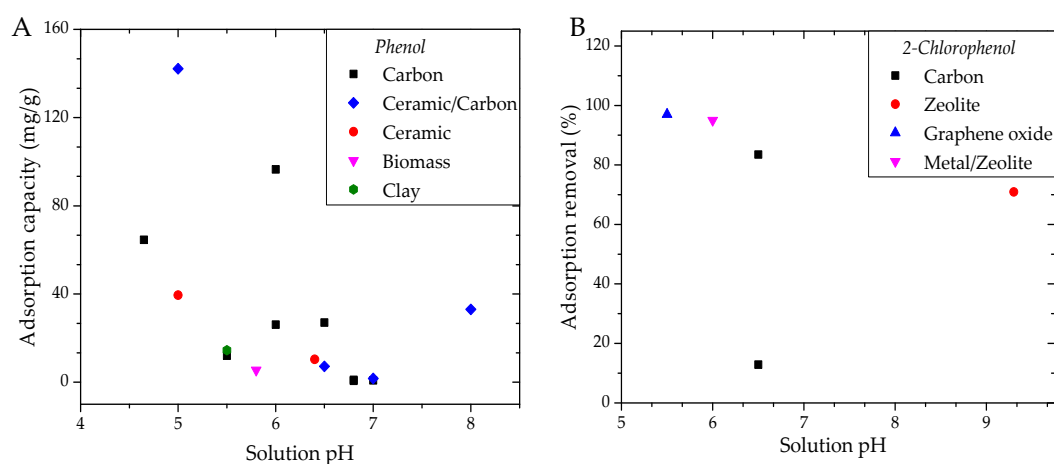


Figure 7. Cont.

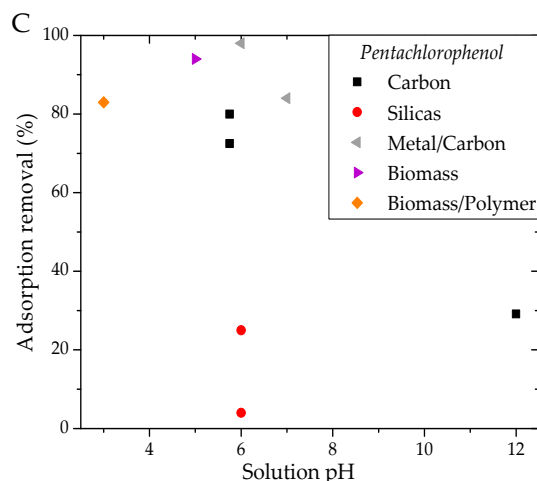


Figure 7. Adsorption performance related to the adsorption test pH for several adsorbents compositions, against Phenol (A); 2-Chlorophenol (B); and Pentachlorophenol (C).

Horseradish peroxidase immobilized on polymer nanofibers was tested in the adsorption of Pentachlorophenol in several solution pH conditions (Table 9, N1). Sorption capacities were reported of 15.27 mg/L, 14.33 mg/L and 11.85 mg/L for an increasing pH of 2, 3, and 4, with no sorption occurring at pH 5 [78]. This direct proportion to solution acidity can be related to the protonation degree of Pentachlorophenol [78]. Since the hydrophobicity of Pentachlorophenol was found to influence the sorption rate, hydrophobic interactions can be identified as a significant capture mechanism. Other mechanisms reported π - π electron interactions between the Pentachlorophenol benzene ring and π electrons of the ketone group from the polymer molecular skeleton, as well as hydrogen bonding between the polymer ketone groups and Pentachlorophenol hydroxyl group [78].

3.2.4. Kinetic Performance of Nanofiber Adsorbents

Figure 8 shows the relationship between adsorption capacity and reaction equilibrium time for different adsorptive structures against phenol. These graphs aim to show the average shorter equilibrium times (under 5 h) reported for nanostructures compared to macro-adsorbents, as can be noticed in Figure 8A, as well as the yield of higher adsorption capacities for nanofibers compared to other nano-structures, with, for instance, activated carbon nanofibers reaching a capacity of 256.1 mg/g after 1.3 h (Table 7, N20). The difference in adsorptive performance and kinetics can be explained by the stability of nanofibers in water, while nanoparticle adsorbents tend to agglomerate under the effect of surface interactions such as Van der Waals, hence hindering the adsorption reaction. The difference in kinetics between nanofibers and macro-structures can be the result of the higher surface to volume ratio of nanofibers. Figure 8B details the composition of the reported adsorbents, revealing a combination of faster kinetics and higher performance for carbonaceous adsorbents, hence suggesting electron interaction as the most efficient predominant adsorption mechanism in the capture of phenol [91].

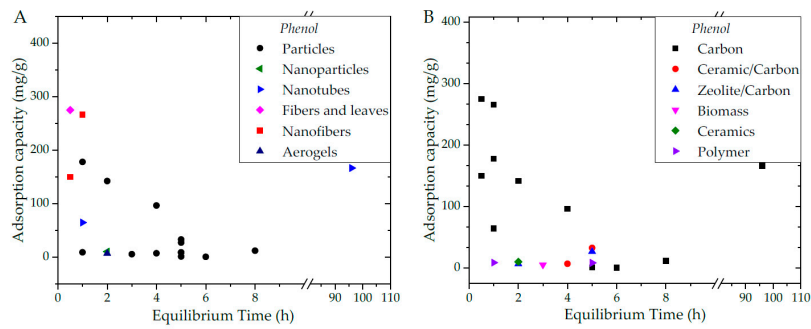


Figure 8. Adsorption performance related to the adsorption test equilibrium time against Phenol, for several adsorbent structures (A) and compositions (B).

3.2.5. Nanofiber Performance Comparison Regarding Initial Contaminant Concentration and Adsorbent Dose

Figure 9 shows bar charts representing the adsorption capacity with the corresponding test conditions of initial disinfectant concentration and adsorbent dose for each nanofiber adsorbent and selected benchmark adsorbents. Comparatively to relatively hydrophilic pesticides, nanofiber adsorbents demonstrated an adsorption capacity in the range of the one performed by activated carbon adsorbents, yet for a lower adsorbent dose. For instance, in the case of phenol capture, activated carbon treated with potassium permanganate demonstrated a capacity of 142.15 mg/g for a contamination of 100 mg/L and a dose of 1 g/L (Table 7, N6). For the same initial contamination, activated carbon microfiber–nanofiber composites showed a capacity of 150 mg/g for a dose of 0.6 g/L (Table 7, N16). It can be seen from all charts that carbon-based adsorbents are amongst the best against phenol and chlorophenols.

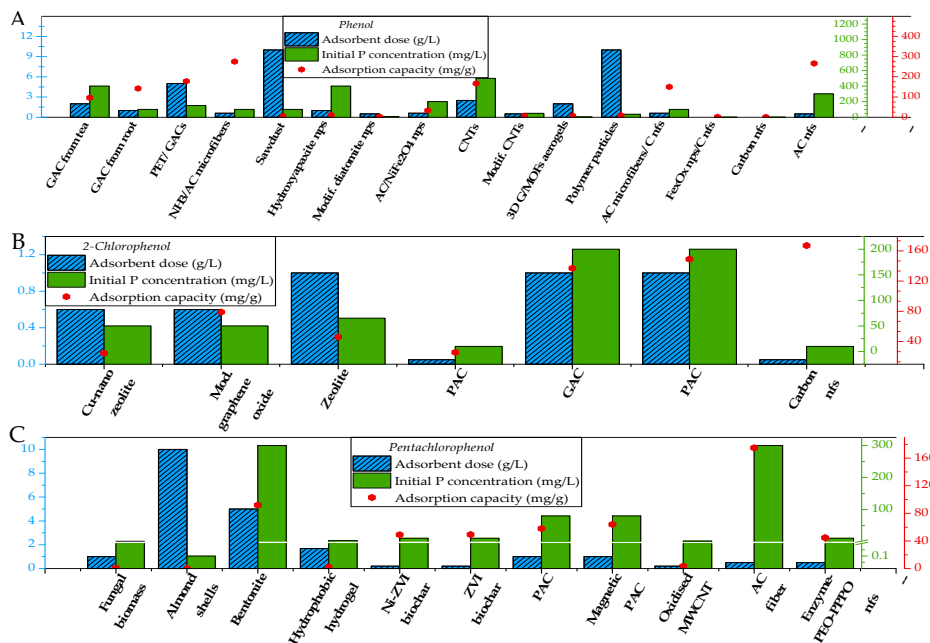


Figure 9. Relationship between adsorbent dose (blue column, left scale), initial pesticide concentration (green column, middle right scale) and adsorption capacity (red scatter, far left scale) in the adsorption of Phenol (A); 2-Chlorophenol (B) and Pentachlorophenol (C).

4. Persistent Organic Pollutants

In this section, the adsorptive performance of nanofiber-based adsorbents is benchmarked and reviewed for the capture of selected aliphatic organochlorines, and selected aromatic compounds from the PCBs and PAHs families. Adsorbate molecules considered in this section are classified POPs (persistent pesticides) and industrial products. Characteristics of the adsorbate shall first be discussed, followed by reported adsorbent structure-performance relationships.

4.1. Aliphatic Organochlorines

4.1.1. Adsorbate Properties

Table 10 shows the physico-chemical characteristics of selected aliphatic organochlorines in this review, namely Aldrin, Dieldrin, Endrin, Chlordane, Heptachlor, Heptachlor epoxide, and Toxaphene 8. Drin pesticides possess an alicyclic structure with 6 chlorine groups. The Aldrin molecule is formed by reaction of norbornadiene, a bicyclic hydrocarbon, and hexachlorocyclopentadiene, also called C-56. In specific conditions, such as in living organisms, Aldrin can be oxidised to form Dieldrin. Endrin is a stereoisomer of Dieldrin, differing in the spatial orientation of the oxygen group, as well as one hydrogen and one chlorine bond. Cyclodiene compounds selected in this study also comprise Chlordane and Heptachlor. Also derived from hexachlorocyclopentadiene, Chlordane and Heptachlor have eight and seven chlorine atoms, respectively, surrounding the polycyclic organic structure. It has been observed that when Heptachlor penetrates the soil, it can be turned into Heptachlor epoxide by soil microorganisms in an epoxy reaction. Toxaphene is another polycyclic organochlorine compound, formed by the chlorination of camphene, usually by chlorine gas. Also called camphechlor or polychlorocamphene, Toxaphene 8 possesses eight chlorine groups [26].

Except for Toxaphene, all molecules present one unsaturated bond, enabling adsorption via π - π stacking of electrons with suitable adsorbents. Dieldrin and Endrin present three chlorine groups at proximity, while other molecules show two chlorine groups, except for Aldrin, which does not show any hydrophobic group near the unsaturated bond.

Selected organochlorine POPs are of a similar weight, ranging from 365 g/mol for Aldrin to 414 g/mol for Toxaphene; however, they differ in their spatial orientation. Apolar molecules have a solubility in water below 0.6 mg/L, with octanol-water partition coefficients over 5. Dieldrin, Endrin and Heptachlor epoxide are only slightly polar molecules due to the presence of one oxygen group (an electron acceptor group), which significantly improves their water affinity (0.019 mg/L for Aldrin and 0.19 mg/L for Dieldrin) and is believed to improve binding with adsorbents by electrostatic interaction.

Table 10. Characteristics of Aldrin, Dieldrin, Endrin, Chlordane, Heptachlor, Heptachlor epoxide, Toxaphene 8 [26].

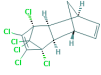
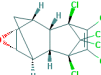
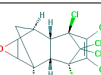
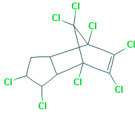
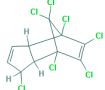
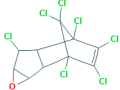
Name	Molecular		Log K_{ow}	Solubility in Water (mg/L, 25 °C)	2D Structure	H Bound Count	
	Weight (g/mol)	Formula				Donor	Acceptor
Aldrin	364.896	C ₁₂ H ₈ Cl ₆	5.6	0.027		0	0
Dieldrin	380.895	C ₁₂ H ₈ Cl ₆ O	5.4	0.19		0	1
Endrin	380.895	C ₁₂ H ₈ Cl ₆ O	5.2	0.23		0	1

Table 10. Cont.

Name	Molecular		Log K _{ow}	Solubility in Water (mg/L, 25 °C)	2D Structure	H Bound Count	
	Weight (g/mol)	Formula				Donor	Acceptor
Chlordane	409.758	C ₁₀ H ₆ Cl ₈	5.16	0.1		0	0
Heptachlor	373.3	C ₁₀ H ₅ Cl ₇	6.10	0.18		0	0
Heptachlor epoxide	389.299	C ₁₀ H ₅ Cl ₇ O	5.40	0.35		0	1
Toxaphene 8	413.79	C ₁₀ H ₁₀ Cl ₈	5.9	0.55		0	0

4.1.2. Nanofibers for Pesticide Adsorption

Figure 10 shows the relationship between adsorption capacity and test conditions of initial contaminant concentration and adsorbent dose for Aldrin, Dieldrin, Endrin pesticides plus Heptachlor and its epoxide. Polystyrene (PES) nanofibers decorated with titania nanoparticles showed limited adsorptive performance for these pesticides, as well as against Chlordane, showing a capacity of 0.02 mg/g (Table 11, N1) [92]. Adsorbent surface properties were not reported, yet the poor affinity of hydrophobic polyester for hydrophobic organochlorines could have impacted the performance, with adsorption reaction localized on the titania surface. In the case of Dieldrin removal, bromopropyl functionalised silica nanofibers revealed an adsorption capacity of 0.19 mg/g for contamination and adsorbent dose of 20 µg/L and 0.1 g/L, respectively (Table 12, N1). In comparison, untreated silica nanofibers achieved a capacity of 0.014 mg/g (Table 12, N2). The addition of a dense bromopropyl layer on silica nanofibers produced a hydrophobic adsorbent surface, with chemical affinity with pesticide chlorine groups.

Concerning Aldrin removal, vegetal activated carbon showed a relatively high performance with a capacity of 0.38 mg/g for a contamination of 2 mg/L, yet for a relatively large dose of 5 g/L (Table 13, N2). Vegetal activated carbon performed a similar role in the case of Dieldrin adsorption, in the same conditions (Table 12, N8). Against Heptachlor epoxide, the vegetal activated carbon was reported to show a capacity of 0.42 mg/g for a contamination of 2.2 mg/L for a similar dose of 5 g/L (Table 14, N7). Finally, in the case of Endrin, powdered activated carbon was reported to show a capacity of 0.085 mg/g for a contamination of 0.8 µg/L, and a relatively large dose of 0.2 g/L (Table 15, N6). These results show that although adsorbent specific surface area and pore channels could be adapted to improve the adsorptive performance, activated carbons yield removal efficiencies over 95%. However, compared to nanomaterial adsorbents, a large adsorbent dose is required.

Acid-treated date and olive stones showed a significantly improved performance over non-treated biomass adsorbents. For instance, acid-treated date stones showed a capacity of 0.45 mg/g in the removal of Aldrin, while untreated date stones yielded 0.05 µg/g for conditions of contamination and adsorbent dose of respectively 500 µg/L, 1 g/L and 0.5 µg/L and 10 g/L (Table 13, N9, N12). Date stones were thermally treated with hydrochloric acid, thus creating a hydrophobic layer on the adsorbent surface, and facilitating the anchorage of organochlorines [93]. In the adsorption of Dieldrin and Endrin, acid-treated date stones showed a capacity of 0.44 mg/g and 0.40 mg/g, in the same conditions as Aldrin capture (Table 12, N18 and Table 15, N10). The lower performance in the adsorption of Endrin compared to Dieldrin can be explained by the spatial organization of

the Endrin molecule, with several orientations. The similar adsorption capacities of Aldrin and Dieldrin indicate that the pesticide oxide groups of Dieldrin and Endrin do not significantly influence the adsorption reaction, meaning electrostatic interactions played a minor role in the capture of these pesticides. Finally, cellulose nanofibers modified with manganese oxide have been reported to yield 96.5% removal against Toxaphene 8, highlighting the potential of metal oxide-based nanofiber adsorbents (Table 16, N1).

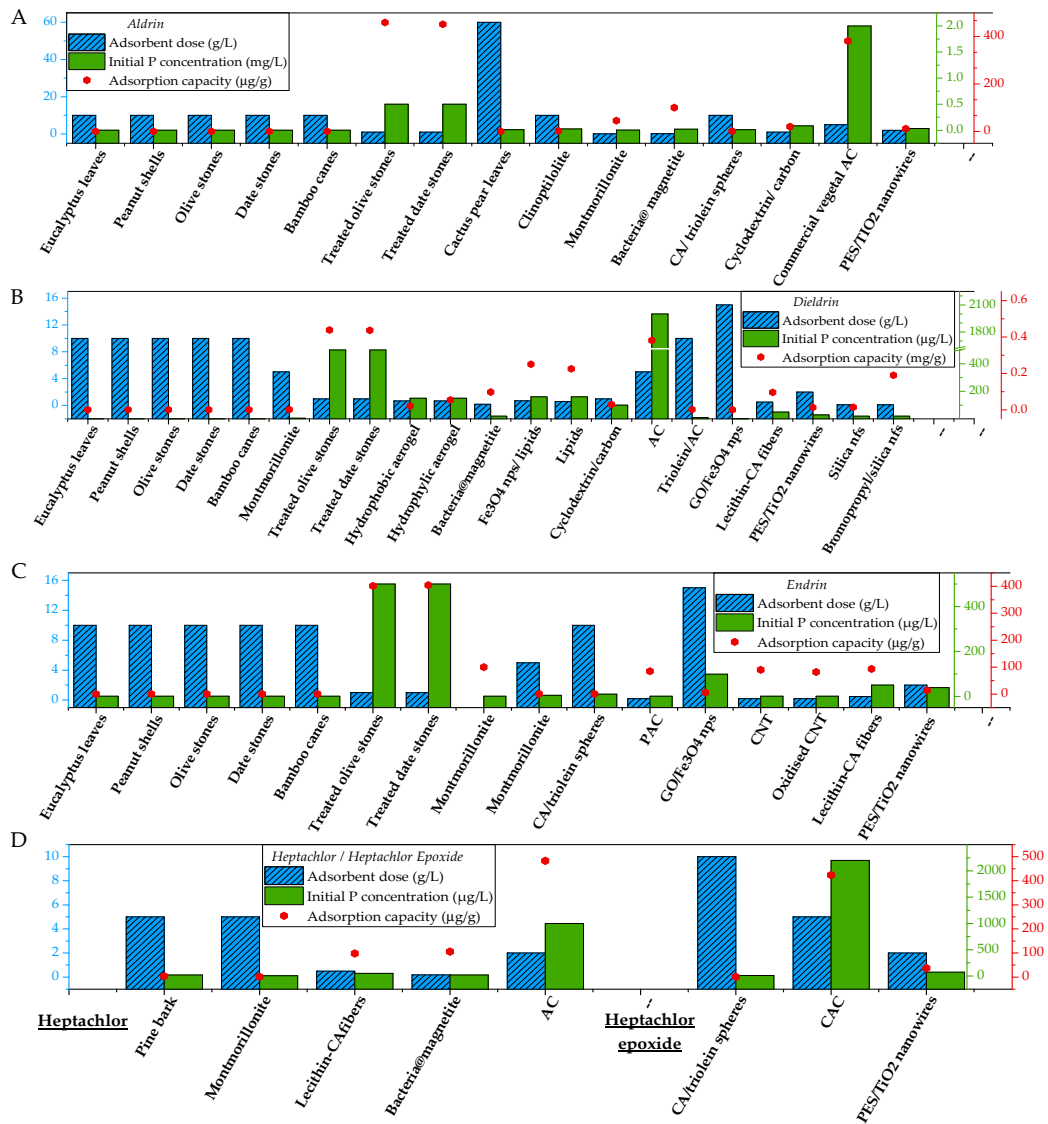


Figure 10. Relationship between adsorbent dose (blue column, left scale), initial pesticide concentration (green column, middle right scale) and adsorption capacity (red scatter, far left scale) in the adsorption of Aldrin (A); Dieldrin (B); Endrin (C); and Heptachlor/epoxide (D). Insufficient data reported for Chlordane and Toxaphene.

Table 11. Nanofibrous adsorbent properties and adsorption conditions for the removal of Chlordane.

N	Adsorbent	Adsorbent Properties			Adsorption Capacity (mg/g)	Initial P Concentration (µg/L)	Adsorbent Dose (g/L)	Adsorption Conditions					Removal (%)	Ref.
		BET (m ² /g)	Pore Volume (cm ³ /g)	Pore Diameter (nm)				pH	Temperature (°C)	Eq. Time (h)	Kinetic Model	Isotherm Model		
1	TiO ₂ nanowires/Polystyrene nanocomposites				0.021	57	2						73.7	[92]

Table 12. Nanofibrous adsorbent properties and adsorption conditions for the removal of Dieldrin.

N	Adsorbent	Adsorbent Properties			Adsorption Capacity (mg/g)	Initial P Concentration (µg/L)	Adsorbent Dose (g/L)	Adsorption Conditions					Removal (%)	Ref.
		BET (m ² /g)	Pore Volume (cm ³ /g)	Pore Diameter (nm)				pH	Temperature (°C)	Eq. Time (h)	Kinetic Model	Isotherm Model		
1	Bromopropyl-silica nanofibers				0.19	20	0.1		25	8		Freundlich	91.0	[94]
2	Silica nanofibers				0.014	20	0.1		25	8			20.9	
3	TiO ₂ nanowires/Polystyrene nanocomposites				0.013	29	2						89.7	[92]
4	Lecithin-Cellulose acetate fibers				0.096	50	0.5			10			96	[95]
5	Graphene oxide-iron oxide nanoparticles				0.00005	1	15	4	25	0.5	Pseudo II order	Langmuir	74	[96]
6	Commercial granulated activated carbon				0.073	20	0.1		25	8			38.7	[94]
7	Triolein embedded activated carbon	721			0.0019	10	10			10				[97]
8	Commercial vegetal activated carbon				0.38	2000	5		20	0.3		Freundlich	95.3	[98]
9	Cyclodextrin-modified nanoporous carbon	890	1.35	5.1	0.03	100	1					Freundlich	30	[99]
10	Cellulose acetate/triolein spheres				0.00095	10	10		25	13			95	[100]
11	Cerasome forming lipid				0.23	160	0.6	7	25			Langmuir	84.4	[101]
12	Cerasome forming lipid with Fe ₃ O ₄ nanoparticles				0.25	160	0.7	7	25			Langmuir	99.9	[101]
13	Bacterial cells adsorbed to magnetite				0.097	20	0.185			0.25			89.9	[102]
14	Hydrophilic silica aerogel	547	2.4	17.6	0.054	150	0.67		25	22			21.5	[103]
15	Hydrophobic silica aerogel	907	2.95	21	0.021	150	0.67		25	6		Freundlich	92.3	[103]
16	Xerogel	988	0.64	3.2	0.0067	150	0.67		25	22			3.0	[103]
17	Cactus pear leaves				0.0001	10	60	7	23	0.15			60	[104]
18	Acid-treated date stones	421			0.44	500	1		25	4.2	Pseudo II order	Freundlich	87.2	[93]
19	Acid-treated olive stones	479			0.44	500	1		25	5	Pseudo II order	Langmuir	87.6	[105]
20	Montmorillonite	18.5			0.00099	5	5	1	25	2	Pseudo II order	Freundlich	99	[106]
21	Bamboo canes	3818			0.000044	0.5	10	6	40	7	Pseudo I order	Freundlich	86.2	[16]
22	Date stones	394.3			0.000041	0.5	10	6	40	7	Pseudo I order	Freundlich	83.9	[16]
23	Olive stones	379.1			0.000047	0.5	10	6	40	7	Pseudo I order	Freundlich	94.9	[16]
24	Peanut shells	367.8			0.00004	0.5	10	6	40	7	Pseudo I order	Freundlich	80.4	[16]
25	Avocado stones	342.2			0.000048	0.5	10	6	40	7	Pseudo I order	Freundlich	95.8	[16]
26	<i>Eucalyptus gomphocephala</i>	289.5			0.000025	0.5	10	6	40	7	Pseudo I order	Freundlich	49.9	[16]
27	<i>Raphanus raphanistrum</i>	296.2			0.000045	0.5	10	6	40	7	Pseudo I order	Freundlich	89.4	[16]
28	<i>Nerium oleander</i>	275.0			0.000037	0.5	10	6	40	7	Pseudo I order	Freundlich	72.8	[16]
29	<i>Origanum compactum</i>	306.3			0.000043	0.5	10	6	40	7	Pseudo I order	Freundlich	87.4	[16]
30	<i>Cistus ladaniferus</i>	311.4			0.000045	0.5	10	6	40	7	Pseudo I order	Freundlich	90.9	[16]

Table 13. Nanofibrous adsorbent properties and adsorption conditions for the removal of Aldrin.

N	Adsorbent	Adsorbent Properties			Adsorption Capacity (mg/g)	Adsorption Conditions						Removal (%)	Ref.	
		BET (m ² /g)	Pore Volume (cm ³ /g)	Pore Diameter (nm)		Initial P Concentration (µg/L)	Adsorbent Dose (g/L)	pH	Temperature (°C)	Eq. Time (h)	Kinetic Model			Isotherm Model
1	TiO ₂ nanowires/Polystyrene nanocomposites				0.011	34	2						64.7	[92]
2	Commercial vegetal activated carbon				0.38	2000	5		20	0.3			95.3	[98]
3	Cyclodextrin modified nanoporous carbon	890	1.35	5.1	0.02	85	1					Freundlich	23.5	[99]
4	Cellulose acetate/triolein spheres				0.001	10	10		25	3			99.9	[100]
5	Bacterial cells adsorbed to magnetite				0.10	20	0.185			0.25			92.9	[102]
6	Montmorillonite	18.5			0.045	5	0.1	6	25	3.75	Pseudo II order	Freundlich	90	[106]
7	Clinoptilolite				0.0023	25	10		25		Pseudo II order	Freundlich	95	[107]
8	Cactus pear leaves				0.0001	10	60	7	23	0.15			60	[104]
9	Acid-treated date stones	421			0.45	500	1		25	4.2	Pseudo II order	Freundlich	90.2	[93]
10	Acid-treated olive stones	479			0.46	500	1		25	5	Pseudo II order	Langmuir	91.7	[105]
11	Bamboo canes	381.8			0.000047	0.5	10	6	40	7	Pseudo I order	Freundlich	93.7	[16]
12	Date stones	394.3			0.000048	0.5	10	6	40	7	Pseudo I order	Freundlich	95.9	[16]
13	Olive stones	379.1			0.000049	0.5	10	6	40	7	Pseudo I order	Freundlich	98.5	[16]
14	Peanut shells	367.7			0.000047	0.5	10	6	40	7	Pseudo I order	Freundlich	94.9	[16]
15	Avocado stones	342.2			0.000049	0.5	10	6	40	7	Pseudo I order	Freundlich	97.4	[16]
16	<i>Eucalyptus gomphocephala</i>	289.5			0.000047	0.5	10	6	40	7	Pseudo I order	Freundlich	93.3	[16]
17	<i>Raphanus raphanistrum</i>	296.2			0.000045	0.5	10	6	40	7	Pseudo I order	Freundlich	90.5	[16]
18	<i>Nerium oleander</i>	275.0			0.000047	0.5	10	6	40	7	Pseudo I order	Freundlich	93.0	[16]
19	<i>Origanum compactum</i>	306.3			0.000046	0.5	10	6	40	7	Pseudo I order	Freundlich	92.3	[16]
20	<i>Cistus landaniferus</i>	311.4			0.000046	0.5	10	6	40	7	Pseudo I order	Freundlich	91.4	[16]

Table 14. Nanofibrous adsorbent properties and adsorption conditions for the removal of Heptachlor and Heptachlor epoxide.

N	Adsorbent	Adsorbent Properties			Adsorption Capacity (mg/g)	Adsorption Conditions						Removal (%)	Ref.	
		BET (m ² /g)	Pore Volume (cm ³ /g)	Pore Diameter (nm)		Initial P Concentration (µg/L)	Adsorbent Dose (g/L)	pH	Temperature (°C)	Eq. Time (h)	Kinetic Model			Isotherm Model
Heptachlor														
1	Activated carbon from wheat straw	176	0.631		0.48	1000	2	7	22	22	Pseudo II order	Langmuir	96.6	[108]
2	Bacterial cells adsorbed to magnetite				0.11	20	0.185			0.25			90.8	[102]
3	Lecithin–Cellulose acetate fibers				0.098	50	0.5			10			98	[95]
4	Montmorillonite	18.5			0.00096	5	5	1	25	2	Pseudo II order	Freundlich	96	[106]
5	Pine bark				0.0038	20	5		20	1.5		Freundlich	93.6	[109]
Heptachlor epoxide														
6	TiO ₂ nanowires/Polystyrene nanocomposites				0.037	74	2						99.9	[92]
7	Commercial vegetal activated carbon				0.42	2200	5		20	0.3			96.4	[98]
8	Cellulose acetate/triolein spheres				0.0009	10	10		25	13			90	[100]

Table 15. Nanofibrous adsorbent properties and adsorption conditions for the removal of Endrin.

N	Adsorbent	Adsorbent Properties			Adsorption Capacity (mg/g)	Adsorption Conditions						Removal (%)	Ref.		
		BET (m ² /g)	Pore Volume (cm ³ /g)	Pore Diameter (nm)		Initial P Concentration (µg/L)	Adsorbent Dose (g/L)	pH	Temperature (°C)	Eq. Time (h)	Kinetic Model			Isotherm Model	
1	TiO ₂ nanowires/Polystyrene nanocomposites				0.014	39	2						71.8	[92]	
2	Lecithin–Cellulose acetate fibers				0.094	50	0.5					10	93.5	[95]	
3	Oxidized carbon nanotubes				0.082	0.8	0.2	6	20				Linear	99.9	[20]
4	Carbon nanotubes	110			0.09	0.8	0.2	6	20				Linear	99.9	[20]
5	Graphene oxide- iron oxide nanoparticles				0.0057	99	15	4	25	0.5		Pseudo I order	Langmuir	86	[96]
6	Powdered activated carbon	742.9			0.085	0.8	0.2	6	20				Linear	99.9	[20]
7	Cellulose acetate/triolein spheres				0.0009	10	10		25	20				90	[100]
8	Montmorillonite	18.5			0.00084	5	5	1	25	2		Pseudo II order	Freundlich	84	[106]
9	Montmorillonite	14.1	0.038	10.9	0.1	1		6.4	20	24			Linear		[110]
10	Acid-treated date stones	421			0.40	500	1		25	4.2		Pseudo II order	Freundlich	80.8	[93]
11	Acid-treated olive stones	479			0.40	500	1		25	5		Pseudo II order	Langmuir	80.2	[105]
12	Bamboo canes	381			0.000042	0.5	10	6	40	7		Pseudo I order	Freundlich	83.0	[16]
13	Date stones	394.			0.000035	0.5	10	6	40	7		Pseudo I order	Freundlich	69.3	[16]
14	Olive stones	379			0.000046	0.5	10	6	40	7		Pseudo I order	Freundlich	92.9	[16]
15	Peanut shells	368			0.000039	0.5	10	6	40	7		Pseudo I order	Freundlich	78.8	[16]
16	Avocado stones	342			0.000048	0.5	10	6	40	7		Pseudo I order	Freundlich	95.9	[16]
17	<i>Eucalyptus gomphocephala</i>	289			0.000039	0.5	10	6	40	7		Pseudo I order	Freundlich	78.5	[16]
18	<i>Raphanus raphanistrum</i>	296			0.000041	0.5	10	6	40	7		Pseudo I order	Freundlich	81.9	[16]
19	<i>Nerium oleander</i>	275			0.000025	0.5	10	6	40	7		Pseudo I order	Freundlich	49.3	[16]
20	<i>Origanum compactum</i>	306			0.000030	0.5	10	6	40	7		Pseudo I order	Freundlich	60.7	[16]
21	<i>Cistus landaniferus</i>	311			0.000037	0.5	10	6	40	7		Pseudo I order	Freundlich	73.4	[16]

Table 16. Nanofibrous adsorbent properties and adsorption conditions for the removal of Toxaphene 8.

N	Adsorbent	Adsorbent Properties			Adsorption Capacity (mg/g)	Adsorption Conditions						Removal (%)	Ref.		
		BET (m ² /g)	Pore Volume (cm ³ /g)	Pore Diameter (nm)		Initial P Concentration (µg/L)	Adsorbent Dose (g/L)	pH	Temperature (°C)	Eq. Time (h)	Kinetic Model			Isotherm Model	
1	MnO ₂ /Cellulose fiber nanocomposites	87			0.965	5000	5	3	25	0.5		Pseudo II order	Langmuir	96.5	[111]

4.2. Polychlorinated Biphenyls (PCBs) and Polyaromatic Hydrocarbons (PAHs)

4.2.1. Adsorbate Properties

Table 17 presents the different molecular structures for the selected polychlorinated biphenyls PCBs in this study, which are namely 2 to 6-PCB, PCB 28 and PCB 77. PCBs are polycyclic aromatic organochlorines of chemical formula $C_{12}H_{10-x}Cl_x$. The PCB structure is composed of two benzene rings, thus sharing the aromatic structure of phenols molecules, and decorated by a number of chlorine groups. PCBs 2 and 3, also called 2- and 3-chlorobiphenyls, possess one chlorine group attached on position 2 and 3, respectively, on one of the benzene rings. Sharing a molecular weight of 188.7 g/mol, water solubility was determined at 1.45 mg/L (25 °C), corresponding to a Log K_{ow} of 4.54. PCBs 4–6 possess two chlorine groups, for a weight of 223.1 g/mol. Their chemical names are 2,2'- 2,3- and 2,3'-dichlorobiphenyls, respectively, corresponding to the chlorine groups' respective positions on one or both benzene rings. PCB 28, called 2,4,4'-trichlorobiphenyl, possesses three chlorine groups for a weight of 257.5 g/mol. PCB 77, called 3,3',4,4'-tetrachlorobiphenyl, possesses four chlorine group for a weight of 292.0 g/mol. Compared to monochloro-biphenyls, PCB 77 water solubility decreased to 0.18 mg/L (25 °C, log K_{ow} 6.72). All molecules are apolar.

Table 17. Molecular structure of PCB 2, PCB 3, PCB 4, PCB 5, PCB 6, PCB 28, and PCB 77 (obtained from PubChem).

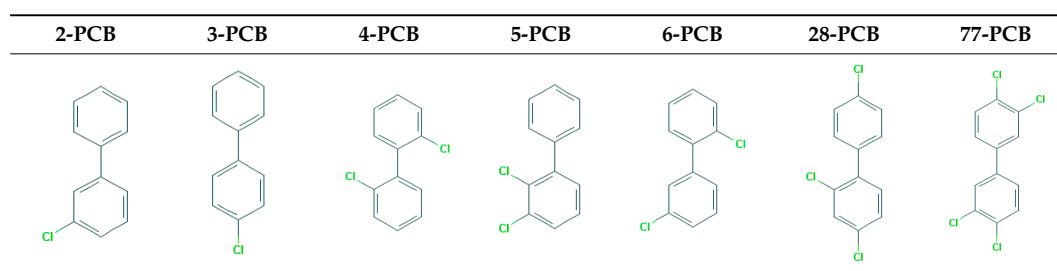
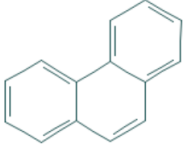


Table 18 presents selected characteristics of the Phenantrene molecule, non-POP-classified, from the family of polycyclic aromatic hydrocarbon compounds. Of a molecular weight in the same order as monochlorinated biphenyls, its water solubility was determined to be 1.15 mg/L (25 °C). An apolar molecule, Phenantrene is composed of three fused benzene rings.

Table 18. Characteristics of Phenantrene (obtained from PubChem).

Name	Formula	M (g/mol)	Log K_{ow}	Solubility in Water (mg/L, 25°C)	Structure
Phenantrene	$C_{14}H_{10}$	178.234	4.46	1.15	

4.2.2. Nanofibers for Pesticide Adsorption

Figure 11 shows the adsorption capacity related to the adsorbent dose and initial contamination for adsorbents of PCBs and Phenantrene. Oriented porous magnetite nanofibers were tested in the adsorption of PCB 77 and showed a capacity of 0.18 mg/g in hexane for a contamination of 30 μ g/L and a dose of 0.15 g/L (Table 19, N8). However, activated carbon showed the largest adsorption capacity of 649 mg/g for a contamination of 4 mg/L and a relatively small dose of 0.015 g/L (Table 19, N1). To study the influence of the adsorbate aromatic structure on the adsorption performance, Phenantrene, with three aromatic cycles, has been considered here. Cellulose acetate unmodified

nanofibers showed limited performance in the capture of Phenantrene, which could be due to the hydrophilic nature of cellulose acetate; they are thus poorly adapted for the adsorption of apolar compounds [112]. Cyclodextrin-grafted cellulose acetate nanofibers were tested for the capture of Phenantrene via molecular filtration, by inclusion–complexation of the hydrophobic contaminants in the apolar cyclodextrin cavity [112]. Hydrophobic interactions led to a contaminant removal of 97% (Table 20, N2). Cross-linking of cellulose acetate nanofibers with benzene rings by polybenzoxazine provided a hydrophobic adsorptive structure [113]. The adsorbent benzene rings further enabled π – π interactions with Phenantrene aromatic rings, thus leading to 98.5% contaminant removal (Table 20, N1).

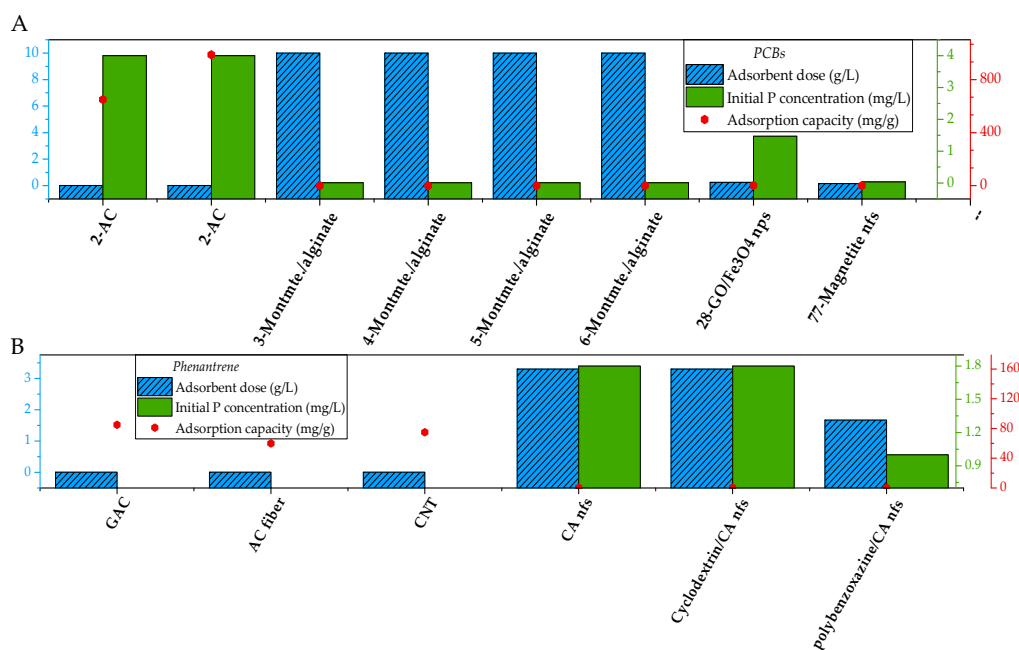


Figure 11. Graphs showing the proportion between adsorbent dose (blue column, left scale), initial pesticide concentration (green column, middle right scale) and adsorption capacity (red scatter, far left scale) in the adsorption of PCBs (A) and Phenantrene (B).

Activated carbons and carbon nanotubes however, demonstrated an adsorption capacity of 85 mg/g for a dose of 4 mg/L (initial concentration was not reported) (Table 20, N7). It can be suggested that π – π electron interaction between the unsaturated Phenantrene aromatics and the carbon adsorbent surface is the predominant reaction mechanism; in that sense, a higher carbon content and full crystalline structure would lead to an increased specific surface area and, for a large pore volume of adapted size, Phenantrene adsorption. Among the reported carbon-based materials, granular activated carbon possessed a BET of 706 m²/g and a pore volume of 0.711 cm³/g, yielding the highest performance. On the other hand, carbon nanotubes with a higher pore volume of 0.818 cm³/g but a lower BET of 537 m²/g showed a capacity of 75 mg/g (Table 20, N4). Furthermore, activated carbon fibers with the highest BET of 949 m²/g but the lowest pore volume of 0.381 cm³/g yielded a lower capacity of 60 mg/g (Table 20, N6), indicating a synergetic effect of pore volume and surface area (BET).

Table 19. Nanofibrous adsorbent properties and adsorption conditions for the removal of PCBs.

N	Adsorbent	Adsorbent Properties			Adsorption Capacity (mg/g)	Adsorption Conditions							Removal (%)	Pesticide	Ref.
		BET (m ² /g)	Pore Volume (cm ³ /g)	Pore Diameter (nm)		Initial P Concentration (µg/L)	Adsorbent Dose (g/L)	pH	Temperature (°C)	Eq. Time (h)	Kinetic Model	Isotherm Model			
1	Activated carbon extracted from coal	986	0.31		649	4000	0.015		25	5			100	PCB 2	[114]
2	Activated carbon extracted from wood	1747	0.48		987	4000	0.015		25	5			100	PCB 2	[114]
3	Montmorillonite clay in alginate gel beads				0.0022	10	10	5.5	25	6.5	Pseudo II order		95	PCB 3	[115]
4	Montmorillonite clay in alginate gel beads				0.0022	10	10	5.5	25	6.5	Pseudo II order		84	PCB 4	[115]
5	Montmorillonite clay in alginate gel beads				0.0019	10	10	5.5	25	6.5	Pseudo II order		79	PCB 5	[115]
6	Montmorillonite clay in alginate gel beads				0.0019	10	10	5.5	25	6.5	Pseudo II order		76	PCB 6	[115]
7	Fe ₃ O ₄ nanoparticles grafted on graphene oxide	145.8			0.71	1470	0.25		25	0.5	Pseudo II order	Linear	12.1	PCB 28	[116]
8	Oriented magnetite porous nanofibers	123		5	0.18	30	0.15			0.1			90.0	PCB-77	[117]

Table 20. Nanofibrous adsorbent properties and adsorption conditions for the removal of Phenantrene.

N	Adsorbent	Adsorbent Properties			Adsorption Capacity (mg/g)	Adsorption Conditions					Removal (%)	Ref.	
		BET (m ² /g)	Diameter (nm)	Pore Volume (cm ³ /g)		Initial P Concentration (mg/L)	Adsorbent Dose (g/L)	Temperature (°C)	Equilibrium Time (h)	Kinetic Model			
1	Cellulose acetate–polybenzoxazine nanofibers		450		0.592	1	1.67			1	Pseudo II order	98.5	[113]
2	Cyclodextrin-grafted cellulose acetate nanofibers		1520		0.52	1.8	3.3			8		97	[112]
3	Cellulose acetate nanofibers		675		0.45	1.8	3.3			3		83	[112]
4	Carbon nanotubes	537		0.818	75		0.004						[112]
5	Benzene-, dextran- and cyclodextrin-coated magnetic nanoparticles				250,000	0.8			25			85	[118]
6	Activated carbon fiber	949		0.381	60		0.004						[112]
7	Granular activated carbon	706		0.711	85		0.004						[112]

5. Adsorbent Regenerability

Two studies reported the adsorbent desorption and recyclability capacity for further use in the industry, and are reviewed below.

Nylon 6–Poly(pyrrole) core-shell nanofibers have been investigated for atrazine desorption and adsorbent regenerability [41]. The desorption procedure consisted of successive washing in methanol and deionized water for 5 min each to elute atrazine, followed by air-drying of nanofibers at room temperature. With this procedure, Nylon-Poly(pyrrole) nanofibers demonstrated the same capacity of 2.77 mg/g over five cycles, with a slight decrease of 0.2 mg/g in adsorption capacity observed at the 6th cycle (Table 4, N3) [41]. With an adsorption plateau reached after 5 h and a desorption procedure estimated around 3 h, such an adsorbent has a life-span of 37 h at its maximal efficiency. Electrostatic interaction and π – π stacking of electrons had been identified as the two adsorption mechanisms at stake in the uptake of Atrazine by Nylon-Poly(pyrrole) nanofibers [41]. Although absorption of Atrazine would be a recyclability limitation, the methanol wash procedure might also imply methanol adsorption.

Manganese oxide–cellulose fiber nanocomposites were investigated for the desorption of Toxaphene (Table 16, N1). Desorption rates were shown to be of 12%, 13% and 25%, respectively, at pH 3, 7, and 11 [111]. The preferential affinity for alkaline pH could suggest the reversibility of the adsorption reaction. Indeed, cellulose and manganese oxide (MnO₂) were reported in the literature to have an isoelectric point of 2.5 and below 5.1, respectively [119,120]. At pH 11, both components of the adsorbent material therefore carry a strong negative surface charge, while the decreasing protonation of Toxaphene with increasing pH could suggest that both adsorbent and adsorbate carry a negative surface charge, hence the desorption. However, the desorption protocol followed was not reported [111].

6. Recommendations and Conclusions

Nanofiber-based materials showed their fast adsorption kinetics and required low adsorbent dose compared to benchmark adsorbents in this study. For instance, polyacrylonitrile nanofibers attained equilibrium after 0.5 h in the adsorption of Atrazine, for an adsorbent dose of 1 g/L (Table 4, N5) [41]. Regarding the adsorption performance, engineered nanofibers yielded over 95% removal efficiency with high adsorption capacities comparable to granular activated carbons and acid-treated biomass. For example, activated carbon nanofibers against Phenol showed a capacity of 256.1 mg/g (Table 7, N20), and cross-linked cellulose acetate-polybenzoxazine nanofibers demonstrated against Phenanthrene 98.5% removal (Table 20, N1) [61,113]. Such a nanofiber web presented adequate structural and chemical surface characteristics for the adsorption of organic contaminants.

Essential structural characteristics for a nanofiber adsorbent were found to be surface pores and density of functional sites. Indeed, the size of pores across the fiber surface was shown to have a major impact on the saturation of the adsorbent, with pore channels engineered to take into account the size or cross section of the contaminant showing higher performance. Activated carbon nanofibers for phenol adsorption present a dual pore repartition of 0.4 nm and 0.8 nm, adapted to the phenol molecule size, with a smallest cross section of 0.43 nm [61]. Molecular orientation of the contaminant is also considered to prevent size-exclusion effects when one molecule is already adsorbed along a pore wall, as highlighted by the performance comparison of Dieldrin and stereoisomer Endrin adsorption [73]. Adsorbent contact surface area ruled by the nanofiber average diameter impacted on the contaminant capture, with diameters below 150 nm yielding higher performance in the capture of Atrazine [39]. Higher surface specific areas led in general to higher adsorption capacities, provided there was contaminant diffusion along the surface pore channels. Activated carbon nanofibers demonstrated a high BET of 2921 m²/g [61].

Regarding adsorbent surface chemistry, a total hydrophobic surface is preferable to show affinity for adsorption—in the case of surface grafting of hydrophobic groups, adsorption may be impeded along the pore walls [28]. Compared to hydrophobic interactions, electrostatic interactions and

foremost electron interactions were shown to be more efficient adsorption mechanisms [41,113]. To this end, adsorbent isoelectric point should be systematically determined to improve the contribution of electrostatic interactions in the contaminant capture. Electron interaction in this study happens via π - π stacking of electrons between adsorbate and adsorbent unsaturated bonds, justifying the high efficiency of carbon-based adsorbents [61]. Other than pore and surface area characteristics, carbon adsorbent crystallinity and carbon content are features of interest that could be investigated in order to improve adsorption by electron interaction. The tuning of the carbon adsorbent surface chemistry to shift its isoelectric point could also be investigated to improve the contaminant adsorption by electrostatic interaction contribution. Other structures such as cellulose acetate crosslinked with polybenzoxazine lead to a highly hydrophobic surface presenting unsaturated bonds, resulting in high performance in the capture of Phenanthrene [113]. Material functionalisation to reach a surface chemistry allowing the three adsorption mechanism defined above could be the focus of future research in order to yield complete contaminant removal.

Testing conditions in terms of initial contaminant concentration were found to vary between 0.5 $\mu\text{g/L}$ and 700 mg/L in this study [16,81]. The initial level of contamination should be justified by the occurrence of the selected contaminant in the environment rather than chosen as a function of the available solution characterisation technique, as adsorbent performance may be affected by a significant change in contaminant concentration. Isotherm analysis was found to be in over 80% of the reported isotherm studies fitted to Langmuir and Freundlich models, with in more than 40% of cases a report of the Freundlich constant with a correlation coefficient below 0.90 for performance comparison with other adsorbents. Adsorption isotherms reflecting the adsorption mechanisms at stake should be more carefully studied to avoid inconsistent performance comparisons.

So far, engineered nanofibers showed the highest performance in the one-off removal of pesticides and disinfectants. However, these adsorbents also show versatility in the capture of contaminants. Ways to create selectivity for a target molecule, such as fiber layers of different pore channels and surface chemistry, could be further investigated. Adsorption being a conventional water treatment technique, the adsorbent material fabrication and operational costs are critical to the implementation of any new classes of materials. Industrial applications of nanofiber adsorbent material solutions should be rigorously assessed and benchmarked against commercially available fabrication routes. The adsorption kinetics and material dosage are also to be considered when evaluating adsorbent life cycle and operational costs. Industrial-scale nanofiber fabrication devices by electrospinning or multi-component fiber extrusion were reported to yield mass output varying between 0.02 kg/h and 0.2 kg/h , and up to 6.5 kg/h , respectively, with a production cost of \$2–5/ kg [121,122]. Other competitive techniques such as force-spinning have been developed to simultaneously increase mass output and fiber quality [123]. Furthermore, to develop a sustainable industry, adsorbent recyclability must be further investigated. As the best-performing materials in the removal of POP may not offer the best recyclability, it is critical to systematically investigate the adsorbent hysteresis of adsorption–desorption. Regeneration of the adsorbent without increasing toxicity concerns linked to adsorbed contaminants must also be investigated.

Acknowledgments: This work was supported by Deakin University and the Australian Research Council with the ARC Linkage Project LP140100374. LD also thanks the ARC for awarding his DECRA 2018 DE180100130 fellowship.

Author Contributions: Elise des Ligneris performed the literature survey, did a major part of the analysis and paper writing. Ludovic F. Dumée contributed in the data analysis and paper writing. Lingxue Kong helped to conceive the paper structure and in the discussion orientation.

Conflicts of Interest: The authors declare no conflict of interest.

References

1. Jones, K.C.; de Voogt, P. Persistent organic pollutants (POPs): State of the science. *Environ. Pollut.* **1999**, *100*, 209–221. [[CrossRef](#)]

2. United Nations Environment Programme (UNEP). Stockholm Convention. Available online: <http://chm.pops.int/> (accessed on 19 September 2017).
3. World Health Organization (WHO). Persistent Organic Pollutants (POPs). Available online: http://www.who.int/foodsafety/areas_work/chemical-risks/pops/en/ (accessed on 19 September 2017).
4. Rashed, M.N. Adsorption technique for the removal of organic pollutants from water and wastewater. In *Organic Pollutants—Monitoring, Risk and Treatment*; Rashed, M.N., Ed.; InTech: Rijeka, Croatia, 2013; Chapter 7.
5. World Health Organization (WHO). *Heptachlor and Heptachlor Epoxide in Drinking-Water*; World Health Organization: Geneva, Switzerland, 2004.
6. Extension Toxicology Network (EXTOXNET). Ddt (Dichlorodiphenyltrichloroethane). Available online: <http://pmep.cce.cornell.edu/profiles/extoxnet/carbaryl-dicropthos/ddt-ext.html> (accessed on 19 September 2017).
7. Wania, F.; MacKay, D. Peer reviewed: Tracking the distribution of persistent organic pollutants. *Environ. Sci. Technol.* **1996**, *30*, 390A–396A. [[CrossRef](#)] [[PubMed](#)]
8. Breivik, K.; Armitage, J.M.; Wania, F.; Sweetman, A.J.; Jones, K.C. Tracking the global distribution of persistent organic pollutants accounting for e-waste exports to developing regions. *Environ. Sci. Technol.* **2016**, *50*, 798–805. [[CrossRef](#)] [[PubMed](#)]
9. Bigot, M.; Muir, D.C.G.; Hawker, D.W.; Cropp, R.; Dachs, J.; Teixeira, C.F.; Bengtson Nash, S. Air–seawater exchange of organochlorine pesticides in the southern ocean between australia and antarctica. *Environ. Sci. Technol.* **2016**, *50*, 8001–8009. [[CrossRef](#)] [[PubMed](#)]
10. Andreozzi, R.; Caprio, V.; Insola, A.; Marotta, R. Advanced oxidation processes (AOP) for water purification and recovery. *Catal. Today* **1999**, *53*, 51–59. [[CrossRef](#)]
11. Gomes, J.; Costa, R.; Quinta-Ferreira, R.M.; Martins, R.C. Application of ozonation for pharmaceuticals and personal care products removal from water. *Sci. Total Environ.* **2017**, *586*, 265–283. [[CrossRef](#)] [[PubMed](#)]
12. Oller, I.; Malato, S.; Sánchez-Pérez, J.A. Combination of advanced oxidation processes and biological treatments for wastewater decontamination—A review. *Sci. Total Environ.* **2011**, *409*, 4141–4166. [[CrossRef](#)] [[PubMed](#)]
13. Köhler, A.; Hellweg, S.; Escher, B.I.; Hungerbühler, K. Organic pollutant removal versus toxicity reduction in industrial wastewater treatment: The example of wastewater from fluorescent whitening agent production. *Environ. Sci. Technol.* **2006**, *40*, 3395–3401. [[CrossRef](#)] [[PubMed](#)]
14. Ellerie, J.R.; Apul, O.G.; Karanfil, T.; Ladner, D.A. Comparing graphene, carbon nanotubes, and superfine powdered activated carbon as adsorptive coating materials for microfiltration membranes. *J. Hazard. Mater.* **2013**, *261*, 91–98. [[CrossRef](#)] [[PubMed](#)]
15. Kakavandi, B.; Jahangiri-rad, M.; Rafiee, M.; Esfahani, A.R.; Babaei, A.A. Development of response surface methodology for optimization of phenol and *p*-chlorophenol adsorption on magnetic recoverable carbon. *Microporous Mesoporous Mater.* **2016**, *231*, 192–206. [[CrossRef](#)]
16. El Bakouri, H.; Morillo, J.; Usero, J.; Ouassini, A. Natural attenuation of pesticide water contamination by using ecological adsorbents: Application for chlorinated pesticides included in european water framework directive. *J. Hydrol.* **2009**, *364*, 175–181. [[CrossRef](#)]
17. Aksu, Z. Application of biosorption for the removal of organic pollutants: A review. *Process Biochem.* **2005**, *40*, 997–1026. [[CrossRef](#)]
18. Bhatnagar, A.; Sillanpää, M. Utilization of agro-industrial and municipal waste materials as potential adsorbents for water treatment—A review. *Chem. Eng. J.* **2010**, *157*, 277–296. [[CrossRef](#)]
19. Rani, M.; Shanker, U.; Jassal, V. Recent strategies for removal and degradation of persistent & toxic organochlorine pesticides using nanoparticles: A review. *J. Environ. Manag.* **2017**, *190*, 208–222.
20. Peng, X.; Jia, J.; Luan, Z. Oxidized carbon nanotubes for simultaneous removal of endrin and Cd(π) from water and their separation from water. *J. Chem. Technol. Biotechnol.* **2009**, *84*, 275–278. [[CrossRef](#)]
21. Shi, B.; Zhuang, X.; Yan, X.; Lu, J.; Tang, H. Adsorption of atrazine by natural organic matter and surfactant dispersed carbon nanotubes. *J. Environ. Sci.* **2010**, *22*, 1195–1202. [[CrossRef](#)]
22. Balamurugan, R.; Sundarajan, S.; Ramakrishna, S. Recent trends in nanofibrous membranes and their suitability for air and water filtrations. *Membranes* **2011**, *1*, 232–248. [[CrossRef](#)] [[PubMed](#)]
23. Ramakrishna, S.; Fujihara, K.; Teo, W.-E.; Yong, T.; Ma, Z.; Ramaseshan, R. Electrospun nanofibers: Solving global issues. *Mater. Today* **2006**, *9*, 40–50. [[CrossRef](#)]

24. Amin, M.T.; Alazba, A.A.; Manzoor, U. A review of removal of pollutants from water/wastewater using different types of nanomaterials. *Adv. Mater. Sci. Eng.* **2014**, *2014*, 24. [CrossRef]
25. Anjum, M.; Miandad, R.; Waqas, M.; Gehany, F.; Barakat, M.A. Remediation of wastewater using various nano-materials. *Arab. J. Chem.* **2016**. [CrossRef]
26. National Center for Biotechnology Information (NCBI). Pubchem. Available online: <https://pubchem.ncbi.nlm.nih.gov/> (accessed on 19 September 2017).
27. Björk, J.; Hanke, F.; Palma, C.-A.; Samori, P.; Cecchini, M.; Persson, M. Adsorption of aromatic and anti-aromatic systems on graphene through π - π stacking. *J. Phys. Chem. Lett.* **2010**, *1*, 3407–3412. [CrossRef]
28. Paul, B.; Martens, W.N.; Frost, R.L. Surface modification of alumina nanofibres for the selective adsorption of alachlor and imazaquin herbicides. *J. Colloid Interface Sci.* **2011**, *360*, 132–138. [CrossRef] [PubMed]
29. Paul, B.; Martens, W.N.; Frost, R.L. Organosilane grafted acid-activated beidellite clay for the removal of non-ionic alachlor and anionic imazaquin. *Appl. Surf. Sci.* **2011**, *257*, 5552–5558. [CrossRef]
30. Faust, S.D.; Aly, O.M. 2-Adsorption models. In *Adsorption Processes for Water Treatment*; Butterworth-Heinemann: Oxford, UK, 1987; pp. 25–64.
31. Chaara, D.; Bruna, F.; Ulibarri, M.A.; Draoui, K.; Barriga, C.; Pavlovic, I. Organo/layered double hydroxide nanohybrids used to remove non ionic pesticides. *J. Hazard. Mater.* **2011**, *196*, 350–359. [CrossRef] [PubMed]
32. Hnatukova, P.; Kopecka, I.; Pivokonsky, M. Adsorption of cellular peptides of microcystis aeruginosa and two herbicides onto activated carbon: Effect of surface charge and interactions. *Water Res.* **2011**, *45*, 3359–3368. [CrossRef] [PubMed]
33. Bosetto, M.; Arfaioli, P.; Fusi, P. Adsorption of the herbicides alachlor and metolachlor on two activated charcoals. *Sci. Total Environ.* **1992**, *123–124*, 101–108. [CrossRef]
34. Behnam, R.; Morshed, M.; Tavanai, H.; Ghiaci, M. Destructive adsorption of diazinon pesticide by activated carbon nanofibers containing Al_2O_3 and mgo nanoparticles. *Bull. Environ. Contam. Toxicol.* **2013**, *91*, 475–480. [CrossRef] [PubMed]
35. Esfandian, H.; Samadi-Maybodi, A.; Parvini, M.; Khoshandam, B. Development of a novel method for the removal of diazinon pesticide from aqueous solution and modeling by artificial neural networks (ANN). *J. Ind. Eng. Chem.* **2016**, *35*, 295–308. [CrossRef]
36. Farmany, A.; Mortazavi, S.S.; Mahdavi, H. Ultrasound-assisted synthesis of $\text{Fe}_3\text{O}_4/\text{SiO}_2$ core/shell with enhanced adsorption capacity for diazinon removal. *J. Magn. Magn. Mater.* **2016**, *416*, 75–80. [CrossRef]
37. Moussavi, G.; Hosseini, H.; Alahabadi, A. The investigation of diazinon pesticide removal from contaminated water by adsorption onto nh_4cl -induced activated carbon. *Chem. Eng. J.* **2013**, *214*, 172–179. [CrossRef]
38. Hassan, A.F.; Elhadidy, H.; Abdel-Mohsen, A.M. Adsorption and photocatalytic detoxification of diazinon using iron and nanotitania modified activated carbons. *J. Taiwan Inst. Chem. Eng.* **2017**, *75*, 299–306. [CrossRef]
39. Peter, K.T.; Vargo, J.D.; Rupasinghe, T.P.; De Jesus, A.; Tivanski, A.V.; Sander, E.A.; Myung, N.V.; Cwiertny, D.M. Synthesis, optimization, and performance demonstration of electrospun carbon nanofiber-carbon nanotube composite sorbents for point-of-use water treatment. *ACS Appl. Mater. Interfaces* **2016**, *8*, 11431–11440. [CrossRef] [PubMed]
40. Ruggieri, F.; D'Archivio, A.A.; Di Camillo, D.; Lozzi, L.; Maggi, M.A.; Mercurio, R.; Santucci, S. Development of molecularly imprinted polymeric nanofibers by electrospinning and applications to pesticide adsorption. *J. Sep. Sci.* **2015**, *38*, 1402–1410. [CrossRef] [PubMed]
41. Yang, B.-Y.; Cao, Y.; Qi, F.-F.; Li, X.-Q.; Xu, Q. Atrazine adsorption removal with nylon6/polypyrrole core-shell nanofibers mat: Possible mechanism and characteristics. *Nanoscale Res. Lett.* **2015**, *10*, 207. [CrossRef] [PubMed]
42. Yan, X.M.; Shi, B.Y.; Lu, J.J.; Feng, C.H.; Wang, D.S.; Tang, H.X. Adsorption and desorption of atrazine on carbon nanotubes. *J. Colloid Interface Sci.* **2008**, *321*, 30–38. [CrossRef] [PubMed]
43. Lupul, I.; Yperman, J.; Carleer, R.; Gryglewicz, G. Adsorption of atrazine on hemp stem-based activated carbons with different surface chemistry. *Adsorption* **2015**, *21*, 489–498. [CrossRef]
44. Zhou, Y.; Zhang, F.; Tang, L.; Zhang, J.; Zeng, G.; Luo, L.; Liu, Y.; Wang, P.; Peng, B.; Liu, X. Simultaneous removal of atrazine and copper using polyacrylic acid-functionalized magnetic ordered mesoporous carbon from water: Adsorption mechanism. *Sci. Rep.* **2017**, *7*, 43831. [CrossRef] [PubMed]

45. Zhang, C.; Zhang, R.Z.; Ma, Y.Q.; Guan, W.B.; Wu, X.L.; Liu, X.; Li, H.; Du, Y.L.; Pan, C.P. Preparation of cellulose/graphene composite and its applications for triazine pesticides adsorption from water. *ACS Sustain. Chem. Eng.* **2015**, *3*, 396–405. [[CrossRef](#)]
46. Suci, N.A.; Capri, E. Adsorption of chlorpyrifos, penconazole and metalaxyl from aqueous solution by modified clays. *J. Environ. Sci. Health Part B* **2009**, *44*, 525–532. [[CrossRef](#)] [[PubMed](#)]
47. Hu, B.; Chen, C.-H.; Frueh, S.J.; Jin, L.; Joesten, R.; Suib, S.L. Removal of aqueous phenol by adsorption and oxidation with doped hydrophobic cryptomelane-type manganese oxide (K–OMS-2) nanofibers. *J. Phys. Chem. C* **2010**, *114*, 9835–9844. [[CrossRef](#)]
48. Srihari, V.; Ashutosh, D. Adsorption of phenol from aqueous media by an agro-waste (*Hemidesmus indicus*) based activated carbon. *Appl. Ecol. Environ. Res.* **2009**, *7*, 13–23. [[CrossRef](#)]
49. Gundogdu, A.; Duran, C.; Senturk, H.B.; Soylak, M.; Ozdes, D.; Serencam, H.; Imamoglu, M. Adsorption of phenol from aqueous solution on a low-cost activated carbon produced from tea industry waste: Equilibrium, kinetic, and thermodynamic study. *J. Chem. Eng. Data* **2012**, *57*, 2733–2743. [[CrossRef](#)]
50. Biglari, H.; Afsharnia, M.; Javan, N.; Sajadi, S.A. Phenol removal from aqueous solutions by adsorption on activated carbon of miswak's root treated with KMnO_4 . *Iran. J. Health Sci.* **2016**, *4*, 20–30. [[CrossRef](#)]
51. Al-Malack, M.H.; Dauda, M. Competitive adsorption of cadmium and phenol on activated carbon produced from municipal sludge. *J. Environ. Chem. Eng.* **2017**, *5*, 2718–2729. [[CrossRef](#)]
52. Gupta, V.K.; Sharma, M.; Singh, K.; Vyas, R.K. Reactive adsorption of phenol onto Fe-GAC: Parallel pore batch modeling and experimental studies. *J. Taiwan Inst. Chem. Eng.* **2016**, *63*, 116–124. [[CrossRef](#)]
53. Haghseresht, F.; Lu, G.Q. Adsorption characteristics of phenolic compounds onto coal-reject-derived adsorbents. *Energy Fuels* **1998**, *12*, 1100–1107. [[CrossRef](#)]
54. Ania, C.O.; Parra, J.B.; Pis, J.J. Effect of texture and surface chemistry on adsorptive capacities of activated carbons for phenolic compounds removal. *Fuel Process. Technol.* **2002**, *77*, 337–343. [[CrossRef](#)]
55. Cheng, W.P.; Gao, W.; Cui, X.; Ma, J.H.; Li, R.F. Phenol adsorption equilibrium and kinetics on zeolite X/activated carbon composite. *J. Taiwan Inst. Chem. Eng.* **2016**, *62*, 192–198. [[CrossRef](#)]
56. Lorenc-Grabowska, E.; Diez, M.A.; Gryglewicz, G. Influence of pore size distribution on the adsorption of phenol on pet-based activated carbons. *J. Colloid Interface Sci.* **2016**, *469*, 205–212. [[CrossRef](#)] [[PubMed](#)]
57. Chakraborty, A.; Deva, D.; Sharma, A.; Verma, N. Adsorbents based on carbon microfibers and carbon nanofibers for the removal of phenol and lead from water. *J. Colloid Interface Sci.* **2011**, *359*, 228–239. [[CrossRef](#)] [[PubMed](#)]
58. Larous, S.; Meniai, A.H. The use of sawdust as by product adsorbent of organic pollutant from wastewater: Adsorption of phenol. *Energy Procedia* **2012**, *18*, 905–914.
59. Arellano-Cárdenas, S.; Gallardo-Velázquez, T.; Osorio-Revilla, G.; del Socorro López-Cortéz, M.; Gómez-Perea, B. Adsorption of phenol and dichlorophenols from aqueous solutions by porous clay heterostructure (PCH). *J. Mex. Chem. Soc.* **2005**, *49*, 287–291.
60. Asmaly, H.A.; Abussaud, B.; Ihsanullah; Saleh, T.A.; Gupta, V.K.; Atieh, M.A. Ferric oxide nanoparticles decorated carbon nanotubes and carbon nanofibers: From synthesis to enhanced removal of phenol. *J. Saudi Chem. Soc.* **2015**, *19*, 511–520. [[CrossRef](#)]
61. Tao, X.; Zhou, G.; Zhuang, X.; Cheng, B.; Li, X.; Li, H. Solution blowing of activated carbon nanofibers for phenol adsorption. *RSC Adv.* **2015**, *5*, 5801–5808. [[CrossRef](#)]
62. Lin, K.; Pan, J.; Chen, Y.; Cheng, R.; Xu, X. Study the adsorption of phenol from aqueous solution on hydroxyapatite nanopowders. *J. Hazard. Mater.* **2009**, *161*, 231–240. [[CrossRef](#)] [[PubMed](#)]
63. Abd El Salam, H.M.; Younis, S.A.; Ali, H.R.; Zaki, T. Statistical modeling and optimization of phenol adsorption from water by modified $\text{Cu}_3(\text{BTC})_2$: Kinetic, isotherm, and thermodynamic analysis. *Microporous Mesoporous Mater.* **2017**, *241*, 210–217. [[CrossRef](#)]
64. Yu, Y.; Hu, Z.; Wang, Y.; Gao, H. Magnetic sn-functionalized diatomite for effective removals of phenols. *Int. J. Miner. Process.* **2017**, *162*, 1–5. [[CrossRef](#)]
65. Changmai, M.; Purkait, M.K. Kinetics, equilibrium and thermodynamic study of phenol adsorption using NiFe_2O_4 nanoparticles aggregated on PAC. *J. Water Process Eng.* **2017**, *16*, 90–97. [[CrossRef](#)]
66. Lin, D.; Xing, B. Adsorption of phenolic compounds by carbon nanotubes: Role of aromaticity and substitution of hydroxyl groups. *Environ. Sci. Technol.* **2008**, *42*, 7254–7259. [[CrossRef](#)] [[PubMed](#)]
67. Soni, U.; Bajpai, J.; Singh, S.K.; Bajpai, A.K. Evaluation of chitosan-carbon based biocomposite for efficient removal of phenols from aqueous solutions. *J. Water Process Eng.* **2017**, *16*, 56–63. [[CrossRef](#)]

68. Han, T.; Xiao, Y.; Tong, M.; Huang, H.; Liu, D.; Wang, L.; Zhong, C. Synthesis of CNT@MIL-68(Al) composites with improved adsorption capacity for phenol in aqueous solution. *Chem. Eng. J.* **2015**, *275*, 134–141. [[CrossRef](#)]
69. Dehghani, M.H.; Mostofi, M.; Alimohammadi, M.; McKay, G.; Yetilmezsoy, K.; Albadarin, A.B.; Heibati, B.; AlGhouti, M.; Mubarak, N.M.; Sahu, J.N. High-performance removal of toxic phenol by single-walled and multi-walled carbon nanotubes: Kinetics, adsorption, mechanism and optimization studies. *J. Ind. Eng. Chem.* **2016**, *35*, 63–74. [[CrossRef](#)]
70. Norzilah, A.H.; Fakhru'l-Razi, A.; Choong, T.S.Y.; Chuah, A.L. Surface modification effects on CNTs adsorption of methylene blue and phenol. *J. Nanomater.* **2011**, *2011*, 18. [[CrossRef](#)]
71. Wang, X.; Lu, M.; Wang, H.; Pei, Y.; Rao, H.; Du, X. Three-dimensional graphene aerogels–mesoporous silica frameworks for superior adsorption capability of phenols. *Separ. Purif. Technol.* **2015**, *153*, 7–13. [[CrossRef](#)]
72. Ipek, I.; Kabay, N.; Yüksel, M. Separation of bisphenol a and phenol from water by polymer adsorbents: Equilibrium and kinetics studies. *J. Water Process Eng.* **2017**, *16*, 206–211. [[CrossRef](#)]
73. Li, X.; Chen, S.; Fan, X.; Quan, X.; Tan, F.; Zhang, Y.; Gao, J. Adsorption of ciprofloxacin, bisphenol and 2-chlorophenol on electrospun carbon nanofibers: In comparison with powder activated carbon. *J. Colloid Interface Sci.* **2015**, *447*, 120–127. [[CrossRef](#)] [[PubMed](#)]
74. Aktaş, Ö.; Çeçen, F. Adsorption, desorption and bioregeneration in the treatment of 2-chlorophenol with activated carbon. *J. Hazard. Mater.* **2007**, *141*, 769–777. [[CrossRef](#)] [[PubMed](#)]
75. Peng, S.; Tang, Z.; Jiang, W.; Wu, D.; Hong, S.; Xing, B. Mechanism and performance for adsorption of 2-chlorophenol onto zeolite with surfactant by one-step process from aqueous phase. *Sci. Total Environ.* **2017**, *581–582*, 550–558. [[CrossRef](#)] [[PubMed](#)]
76. Soltani, T.; Lee, B.-K. Mechanism of highly efficient adsorption of 2-chlorophenol onto ultrasonic graphene materials: Comparison and equilibrium. *J. Colloid Interface Sci.* **2016**, *481*, 168–180. [[CrossRef](#)] [[PubMed](#)]
77. Huong, P.-T.; Lee, B.-K.; Kim, J. Improved removal of 2-chlorophenol by a synthesized Cu-nano zeolite. *Process Saf. Environ. Prot.* **2016**, *100*, 272–280. [[CrossRef](#)]
78. Niu, J.; Xu, J.; Dai, Y.; Xu, J.; Guo, H.; Sun, K.; Liu, R. Immobilization of horseradish peroxidase by electrospun fibrous membranes for adsorption and degradation of pentachlorophenol in water. *J. Hazard. Mater.* **2013**, *246–247*, 119–125. [[CrossRef](#)] [[PubMed](#)]
79. Leyva-Ramos, R.; Diaz-Flores, P.E.; Leyva-Ramos, J.; Femat-Flores, R.A. Kinetic modeling of pentachlorophenol adsorption from aqueous solution on activated carbon fibers. *Carbon* **2007**, *45*, 2280–2289. [[CrossRef](#)]
80. Abdel Salam, M.; Burk, R.C. Thermodynamics of pentachlorophenol adsorption from aqueous solutions by oxidized multi-walled carbon nanotubes. *Appl. Surf. Sci.* **2008**, *255*, 1975–1981. [[CrossRef](#)]
81. Domínguez-Vargas, J.R.; Navarro-Rodríguez, J.A.; de Heredia, J.B.; Cuerda-Correa, E.M. Removal of chlorophenols in aqueous solution by carbon black low-cost adsorbents. Equilibrium study and influence of operation conditions. *J. Hazard. Mater.* **2009**, *169*, 302–308. [[CrossRef](#)] [[PubMed](#)]
82. Devi, P.; Saroha, A.K. Synthesis of the magnetic biochar composites for use as an adsorbent for the removal of pentachlorophenol from the effluent. *Bioresour. Technol.* **2014**, *169*, 525–531. [[CrossRef](#)] [[PubMed](#)]
83. Devi, P.; Saroha, A.K. Simultaneous adsorption and dechlorination of pentachlorophenol from effluent by ni-zvi magnetic biochar composites synthesized from paper mill sludge. *Chem. Eng. J.* **2015**, *271*, 195–203. [[CrossRef](#)]
84. Zhu, D.; Zhang, H.; Tao, Q.; Xu, Z.; Zheng, S. Surface functionalized mesoporous silicas as adsorbents for aromatic contaminants in aqueous solution. *Environ. Toxicol. Chem.* **2009**, *28*, 1400–1408. [[CrossRef](#)] [[PubMed](#)]
85. Yang, B.; Xu, D.; Wu, X.; Li, Z.; Lei, L.; Zhang, X. Efficient removal of pentachlorophenol from wastewater by novel hydrophobically modified thermo-sensitive hydrogels. *J. Ind. Eng. Chem.* **2015**, *25*, 67–72. [[CrossRef](#)]
86. Zhang, Y.; Long, Y.; Yuancheng, Z.; Zhu, Y.; Wang, H.; Wu, H.; Lu, W. Effect of a mixed anionic-nonionic surfactant adsorption on bentonite structure and on distribution of pentachlorophenol. *Appl. Clay Sci.* **2012**, *69*, 93–98. [[CrossRef](#)]
87. Estevinho, B.N.; Ratola, N.; Alves, A.; Santos, L. Pentachlorophenol removal from aqueous matrices by sorption with almond shell residues. *J. Hazard. Mater.* **2006**, *137*, 1175–1181. [[CrossRef](#)] [[PubMed](#)]
88. Mathialagan, T.; Viraraghavan, T. Biosorption of pentachlorophenol from aqueous solutions by a fungal biomass. *Bioresour. Technol.* **2009**, *100*, 549–558. [[CrossRef](#)] [[PubMed](#)]

89. Atieh, M.A. Removal of phenol from water different types of carbon—A comparative analysis. *APCBEE Procedia* **2014**, *10*, 136–141. [[CrossRef](#)]
90. Zhou, Q.; Xu, R. Adsorption of 2,4-dichlorophenol on meta-aramid/poly (acrylic acid) composite nanofibrous membranes. *Adv. Mater. Res.* **2013**, *610–613*, 551–555.
91. Salame, I.I.; Bandoz, T.J. Role of surface chemistry in adsorption of phenol on activated carbons. *J. Colloid Interface Sci.* **2003**, *264*, 307–312. [[CrossRef](#)]
92. Youssef, A.M.; Malhat, F.M.; Abd El-Hakim, A.F.A. Preparation and utilization of polystyrene nanocomposites based on TiO₂ nanowires. *Polym. Plast. Technol. Eng.* **2013**, *52*, 228–235. [[CrossRef](#)]
93. El Bakouri, H.; Usero, J.; Morillo, J.; Rojas, R.; Ouassini, A. Drin pesticides removal from aqueous solutions using acid-treated date stones. *Bioresour. Technol.* **2009**, *100*, 2676–2684. [[CrossRef](#)] [[PubMed](#)]
94. Yue, X.; Feng, S.; Li, S.; Jing, Y.; Shao, C. Bromopropyl functionalized silica nanofibers for effective removal of trace level dieldrin from water. *Colloids Surf. A Physicochem. Eng. Asp.* **2012**, *406*, 44–51. [[CrossRef](#)]
95. Huo, J.; Wang, Y. Preparation and characteristics of novel fibers based on cellulose acetate and soy lecithin for attracting and binding pops. *J. Geosci. Environ. Prot.* **2015**, *3*, 1–8. [[CrossRef](#)]
96. Shrivastava, K.; Ghosale, A.; Nirmalkar, N.; Srivastava, A.; Singh, S.K.; Shinde, S.S. Removal of endrin and dieldrin isomeric pesticides through stereoselective adsorption behavior on the graphene oxide-magnetic nanoparticles. *Environ. Sci. Pollut. Res. Int.* **2017**, *24*, 24980–24988. [[CrossRef](#)] [[PubMed](#)]
97. Jia, R.; Liu, H.; Qu, J.; Qu, A.; Dai, R. Characterization and adsorption behavior of a novel triolein-embedded activated carbon composite adsorbent. *Chin. Sci. Bull.* **2005**, *50*, 2788–2790. [[CrossRef](#)]
98. Bandala, E.R.; Andres-Octaviano, J.; Pastrana, P.; Torres, L.G. Removal of aldrin, dieldrin, heptachlor, and heptachlor epoxide using activated carbon and/or pseudomonas fluorescens free cell cultures. *J. Environ. Sci. Health Part B* **2006**, *41*, 553–569. [[CrossRef](#)] [[PubMed](#)]
99. Zolfaghari, G. B-cyclodextrin incorporated nanoporous carbon: Host-guest inclusion for removal of *p*-nitrophenol and pesticides from aqueous solutions. *Chem. Eng. J.* **2016**, *283*, 1424–1434. [[CrossRef](#)]
100. Liu, H.; Ru, J.; Qu, J.; Dai, R.; Wang, Z.; Hu, C. Removal of persistent organic pollutants from micro-polluted drinking water by triolein embedded adsorbent. *Bioresour. Technol.* **2009**, *100*, 2995–3002. [[CrossRef](#)] [[PubMed](#)]
101. Feng, S.; Ma, F.; Liu, R.; Li, S.; Li, X.; Jin, Y.; Fu, G.; Yue, X. Highly efficient removal of trace level dieldrin from water resources utilizing a cerasomal strategy. *J. Mater. Chem. A* **2016**, *4*, 10263–10273. [[CrossRef](#)]
102. Mac Rae, I.C. Removal of chlorinated hydrocarbons from water and wastewater by bacterial cells adsorbed to magnetite. *Water Res.* **1986**, *20*, 1149–1152. [[CrossRef](#)]
103. Liu, H.; Sha, W.; Cooper, A.T.; Fan, M. Preparation and characterization of a novel silica aerogel as adsorbent for toxic organic compounds. *Colloids Surf. A Physicochem. Eng. Asp.* **2009**, *347*, 38–44. [[CrossRef](#)]
104. Gebrekidan, A.; Nicolai, H.; Vincken, L.; Teferi, M.; Asmelash, T.; Dejenie, T.; Zerabruk, S.; Gebrehiwet, K.; Bauer, H.; Deckers, J.; et al. Pesticides removal by filtration over cactus pear leaves: A cheap and natural method for small-scale water purification in semi-arid regions. *CLEAN Soil Air Water* **2013**, *41*, 235–243. [[CrossRef](#)]
105. El Bakouri, H.; Usero, J.; Morillo, J.; Ouassini, A. Adsorptive features of acid-treated olive stones for drin pesticides: Equilibrium, kinetic and thermodynamic modeling studies. *Bioresour. Technol.* **2009**, *100*, 4147–4155. [[CrossRef](#)] [[PubMed](#)]
106. Ozcan, S.; Tor, A.; Aydin, M.E. An investigation on the sorption behaviour of montmorillonite for selected organochlorine pesticides from water. *Environ. Technol.* **2012**, *33*, 1239–1245. [[CrossRef](#)] [[PubMed](#)]
107. Sprynskyy, M.; Ligor, T.; Buszewski, B. Clinoptilolite in study of lindane and aldrin sorption processes from water solution. *J. Hazard. Mater.* **2008**, *151*, 570–577. [[CrossRef](#)] [[PubMed](#)]
108. Seyhi, B.; Drogui, P.; Gortares-Moroyoqui, P.; Estrada-Alvarado, M.I.; Alvarez, L.H. Adsorption of an organochlorine pesticide using activated carbon produced from an agro-waste material. *J. Chem. Technol. Biotechnol.* **2014**, *89*, 1811–1816. [[CrossRef](#)]
109. Ratola, N.; Botelho, C.; Alves, A. The use of pine bark as a natural adsorbent for persistent organic pollutants—Study of lindane and heptachlor adsorption. *J. Chem. Technol. Biotechnol.* **2003**, *78*, 347–351. [[CrossRef](#)]
110. Peng, X.; Wang, J.; Fan, B.; Luan, Z. Sorption of endrin to montmorillonite and kaolinite clays. *J. Hazard. Mater.* **2009**, *168*, 210–214. [[CrossRef](#)] [[PubMed](#)]

111. Gupta, V.K.; Fakhri, A.; Agarwal, S.; Sadeghi, N. Synthesis of MnO₂/cellulose fiber nanocomposites for rapid adsorption of insecticide compound and optimization by response surface methodology. *Int. J. Biol. Macromol.* **2017**, *102*, 840–846. [CrossRef] [PubMed]
112. Celebioglu, A.; Demirci, S.; Uyar, T. Cyclodextrin-grafted electrospun cellulose acetate nanofibers via “click” reaction for removal of phenanthrene. *Appl. Surf. Sci.* **2014**, *305*, 581–588. [CrossRef]
113. Ertas, Y.; Uyar, T. Fabrication of cellulose acetate/polybenzoxazine cross-linked electrospun nanofibrous membrane for water treatment. *Carbohydr. Polym.* **2017**, *177*, 378–387. [CrossRef] [PubMed]
114. Perrard, A.; Descorme, C. Static and dynamic adsorption studies of polychlorobiphenyls (PCBs) over activated carbons. *Chemosphere* **2016**, *145*, 528–534. [CrossRef] [PubMed]
115. Barreca, S.; Orecchio, S.; Pace, A. The effect of montmorillonite clay in alginate gel beads for polychlorinated biphenyl adsorption: Isothermal and kinetic studies. *Appl. Clay Sci.* **2014**, *99*, 220–228. [CrossRef]
116. Zeng, S.; Gan, N.; Weideman-Mera, R.; Cao, Y.; Li, T.; Sang, W. Enrichment of polychlorinated biphenyl 28 from aqueous solutions using Fe₃O₄ grafted graphene oxide. *Chem. Eng. J.* **2013**, *218*, 108–115. [CrossRef]
117. Han, C.; Cai, W.; Tang, W.; Wang, G.; Liang, C. Protein assisted hydrothermal synthesis of ultrafine magnetite nanoparticle built-porous oriented fibers and their structurally enhanced adsorption to toxic chemicals in solution. *J. Mater. Chem.* **2011**, *21*, 11188–11196. [CrossRef]
118. Cho, E.; Tahir, M.N.; Choi, J.M.; Kim, H.; Yu, J.-H.; Jung, S. Novel magnetic nanoparticles coated by benzene- and β-cyclodextrin-bearing dextran, and the sorption of polycyclic aromatic hydrocarbon. *Carbohydr. Polym.* **2015**, *133*, 221–228. [CrossRef] [PubMed]
119. Morimoto, T.; Kittaka, S. Isoelectric point of manganese oxide. *Bull. Chem. Soc. Jpn.* **1974**, *47*, 2. [CrossRef]
120. Sookne, A.; Harris, M. Surface characteristics of cotton fibers, as indicated by electrophoretic studies. *J. Res. Natl. Bur. Stand.* **1941**, *26*, 65–69. [CrossRef]
121. Electrospintech. Electrospinning Mass Production Output. Available online: <http://electrospintech.com/production-level.html#.Wl2WIGeW58E> (accessed on 15 January 2018).
122. Luo, C.J.; Stoyanov, S.D.; Stride, E.; Pelan, E.; Edirisinghe, M. Electrospinning versus fibre production methods: From specifics to technological convergence. *Chem. Soc. Rev.* **2012**, *41*, 4708–4735. [CrossRef] [PubMed]
123. Sarkar, K.; Gomez, C.; Zambrano, S.; Ramirez, M.; de Hoyos, E.; Vasquez, H.; Lozano, K. Electrospinning to forcespinning™. *Mater. Today* **2010**, *13*, 12–14. [CrossRef]



© 2018 by the authors. Licensee MDPI, Basel, Switzerland. This article is an open access article distributed under the terms and conditions of the Creative Commons Attribution (CC BY) license (<http://creativecommons.org/licenses/by/4.0/>).